Distribution Agreement

In presenting this thesis or dissertation as a partial fulfillment of the requirements for an advanced degree from Emory University, I hereby grant to Emory University and its agents the non-exclusive license to archive, make accessible, and display my thesis or dissertation in whole or in part in all forms of media, now or hereafter known, including display on the world wide web. I understand that I may select some access restrictions as part of the online submission of this thesis or dissertation. I retain all ownership rights to the copyright of the thesis or dissertation. I also retain the right to use in future works (such as articles or books) all or part of this thesis or dissertation.

Signature:

_____

Dongmei Xiang Date

CO_2 Reduction Catalyzed by Mercaptopteridine

By

Dongmei Xiang

Doctor of Philosophy

Chemistry

_____

Dr. Brian R. Dyer
Advisor

_____

Dr. Craig L. Hill
Committee Member

_____

Dr. Tianquan (Tim) Lian
Committee Member

Accepted:

_____

Lisa A. Tedesco, Ph.D.
Dean of the James T. Laney School of Graduate Studies

_____ Date

CO_2 Reduction Catalyzed by Mercaptopteridine

By

Dongmei Xiang

B.S. Xiamen University, Fujian, China, 2010

Advisor: Brian R. Dyer, PhD.

An abstract of

A dissertation submitted to the Faculty of the

James T. Laney School of Graduate Studies of Emory University

in partial fulfillment of the requirements for the degree of

Doctor of Philosophy

in Chemistry

2016

Abstract

CO_2 Reduction Catalyzed by Mercaptopteridine

By Dongmei Xiang

The catalytic reduction of CO_2 is of great interest since it plays a significant role in climate change and the global energy cycle. Inspired by the role of pterin in biological systems as a redox mediator and C1 carrier, we studied 6,7-dimethyl-4-hydroxy-2-mercaptopter 6,7-dimethyl-4-hydroxy-2-mercaptopteridine (PTE) to catalyze CO_2 reduction on the glassy carbon electrode. In bulk electrolysis of a saturated CO_2 solution in the presence of the PTE catalyst, Fourier transform infrared data show the progression of carbamate intermediate and reduced products, including formate, formaldehyde and methanol. ^{13}C NMR spectroscopy and gas chromatography data prove the production of methanol with a Faradaic efficiency of 10−23%. A multiple hydride transfer mechanism is proposed for the progressive multi-electron reduction of CO_2. PTE is proved to catalyze the reduction of CO_2 at low overpotential and without the involvement of any metal.

Photochemical CO_2 reduction was studied by using CdSe quantum dots as a photosensitizer. Transient absorbance spectroscopy in the ultraviolet spectral region proves the electron transfer from quantum dots to PTE catalyst. The photo-generated 1 e^- reduced PTE is formed. However, the active form of catalysis should be the 2 e- reduced PTE, which calls for future work.

CO_2 Reduction Catalyzed by Mercaptopteridine

By

Dongmei Xiang

B.S. Xiamen University, Fujian, China, 2010

Advisor: Brian R. Dyer, PhD.

A dissertation submitted to the Faculty of the

James T. Laney School of Graduate Studies of Emory University

in partial fulfillment of the requirements for the degree of

Doctor of Philosophy

in Chemistry

2016

Acknowledgments

First, I would like to express my gratitude to my advisor Prof. Brian Dyer, who has always been a great source of support and guidance for my whole graduate student life. As a scientist, Dr. Dyer has inspired me by his curiosity, critical thinking, diligence and persistence, which would also benefit me in every aspect of life. I would also like to thank my graduate committee members, Prof. Craig L. Hill and Prof. Tianquan Lian. They are excellent role models and have provided me insightful comments, challenging questions and valuable support.

It is such a pleasure to work in the Dyer lab because of the supportive and adorable lab fellows. I enjoy the fun and fulfilling working environment a lot. I would like to thank the talented Dr. Donny Magana especially, who was such a good mentor in lab and never hesitant to share knowledge and help me grow as a scientist.

I would also like to thank the cute couple Dr. Ye Yang and Dr. Wenting Wu, who picked me up from the airport when I first arrived in Atlanta. Since then, they have been wonderful mentors, helping me adapt to new life as quickly as possible, encouraging me when I was upset, and bringing lots of joy to my life.

Besides, I would like to thank my long list of good friends and they have made my life in Atlanta such a terrific experience.

Finally, I would like to thank my beloved parents and brother, for always standing by my side, supporting me and encouraging me. With their love, I'm fearless.

List of Frequently Used Abbreviations

Abbreviation	Full Name
PTE	6,7-dimethyl-4-hydroxy-2-mercaptopter 6,7-dimethyl-4-hydroxy-2-mercaptopteridine
Pte(II)	2,4-Diamino-6-(hydroxymethyl)pteridine
Py	pyridine
Spy	mercaptopyridine
PyH_2	dihydropyridine
MPT	methanopterin
THF	tetrahydrofuran
EDTA	ethylenediaminetetraacetic acid
QD	quantum dots
GC	glassy carbon electrode
UV-Vis	ultraviolet–visible
NMR	nuclear magnetic resonance spectroscopy
FTIR	Fourier transform infrared spectroscopy
ET	electron transfer
HT	hydride transfer
PT	proton transfer
PCET	proton coupled electron transfer

Table of contents

List of Figures

List of Tables

Chapter 1. Introduction

1.1. The significance and challenge of CO_2 reduction

Humanity is the one of the largest driving forces for changing the earth's climate, and the dominant effect is the increase of greenhouse gases in earth's atmospheric composition, which changes the energy balance on earth. Carbon dioxide is considered to be the one of the leading components of greenhouse gases and a common example of a climate forcing agent.[1,2] It retains heat because it has a large infrared absorption at an open window in the solar spectrum where H_2O has no absorption. CO_2 emission mostly comes from the burning of fossil fuels. Since the industrial revolution, fossil fuels have been essential to provide energy to every part of human society.[3] According to BP's energy outlook (2016), fossil fuels remain the dominant form of energy to power the global expansion: they are predicted to provide around 60% of the additional energy and to account for almost 80% of total energy supplies in 2035. Through the development of new technology, non-standard sources of fossil fuels have become accessible and they are still going to play a major role in the energy profile; this is, however, non-sustainable in terms of carbon emission. Meanwhile, the amount of fossil fuel is not infinite and will decrease with consumption, especially since the world population is growing and the life expectancy is increasing. Therefore, if there is a way to convert the greenhouse gas carbon dioxide to useful fossil fuels, ideally in a carbon neutral way, we can potentially alleviate both energy and climate issues.

Scientists have been studying the utilization of CO_2 for decades. The first important factor is the source of CO_2, which determines the quality including purity and partial pressure, which leads to development of separation and storage technologies.[3]

Then there are multiple ways to utilize CO_2. One is to incorporate CO_2 into organic molecules, which produces carboxylates, carbamates, and carbonates. [4] These reactions, however, are not used to produce bulk fuels or chemicals since there is no large scale implementation and they require a large energy input, resulting in a negative net energy balance. Alternatively, CO_2 can be converted to hydrocarbons as direct functionalization via modified methanol and Fischer-Tropsch synthesis, which can be implemented on a large scale. CO_2 can also be converted into syngas (H_2 + CO), and then used to make liquid fuels through the famous Fischer–Tropsch process under high temperature and pressure, which requires high capital, operation and maintenance costs. Meanwhile, the Fischer-Tropsch process requires an essential reactant H_2, which needs to be cheap and clean to make the Fischer-Tropsch process cost-effective. The hydrogenation of CO_2 via the Fischer–Tropsch process can be summarized as three major steps as shown in Figure 1.1.[5] For all of the processes discussed here, an alternative source of energy is required, because otherwise fossil fuels are still essential to drive these reactions, leading to a net negative energy balance.

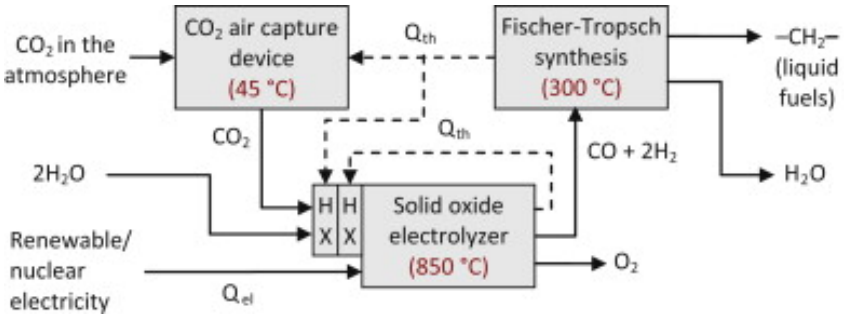

Figure 1.1. Schematic of the proposed CO_2-recycled synthetic fuel production process. –CH_2– represents a hydrocarbon, which could also be represented as a longer chain molecule such as C_8H_{18}. HX: heat exchanger. Adapted with permission from reference 5

Besides direct hydrogenation, there are also electrocatalytic CO_2 reduction and photocatalytic CO_2 conversion. CO_2 is an extremely stable molecule. The reduction of CO_2 is challenging issue because of the slow kinetics and the requirement of a high reduction overpotential.[6] Overpotential is the difference between a half-reaction's thermodynamic reduction potential and the experimentally observed potential of the redox reaction[7]. In an electrolytic cell, high overpotential means it requires more energy than thermodynamically expected to drive a reaction, therefore, overpotential is undesirable.

One reason that CO_2 reduction is slow is that the mechanism may involve high energy intermediates such as the one electron reduced species. As to the single-electron reduction process (eqn. 1) in CO_2 reduction, it requires a large reorganization energy to go from the linear CO_2 molecule to the bent radical anion with a change in hybridization

of the central carbon from sp^2 to sp^3. The large kinetic barrier to this process requires a catalyst to remove[8]. The standard potential for $CO_2/CO_2^{\bullet -}$ is -1.9 V vs. NHE in aqueous solution, which is too negative in terms of energy efficiency. Thus one strategy for catalytic CO_2 reduction is to bypass the formation of high energy $CO_2^{\bullet}$ radical. The thermodynamic barrier can also be reduced by protonating the reduction product.[6b] The redox potentials E°(vs. normal hydrogen electrode, NHE, at pH 7 in aqueous solution, 25 °C) are shown below[9], which indicates that the proton-assisted, multiple electron routes (eqn.2~6) require much less energy than the single electron associated reduction process. The former ones produce thermodynamically more stable products. Hence, there might be a considerable advantage to conduct the multiple electron steps via optimal catalysts to reduce CO_2. Eqn. 7 is the hydrogen evolution reaction, which has a more positive reduction potential compared with the proton-coupled multi-electron CO_2 reduction process of many common products. Thus, the hydrogen evolution reaction is invariably competing with CO_2 reduction in aqueous media and the selectivity and the catalytic selectivity (CS) of CO_2 reduction can be defined as eqn. (8).[10] In most cases, Faradaic efficiency is used to characterize a CO_2 reduction system as in eqn. (9), which is the ratio of charge passed through CO_2 reduction products and total charge passed in an electrochemical reaction.

$$CO_2 + e^- \rightarrow CO_2^{\bullet -} \qquad E° = -1.85\ V \quad (1)$$

$$CO_2 + 2H^+ + 2e^- \rightarrow CO + H_2O \qquad E° = -0.53\ V \quad (2)$$

$$CO_2 + 2H^+ + 2e^- \rightarrow HCO_2H \qquad E° = -0.61\ V \quad (3)$$

$CO_2 + 4H^+ + 4e^- \rightarrow HCHO + H_2O$ $E°= -0.48$ V (4)

$CO_2 + 6H^+ + 6e^- \rightarrow CH_3OH + H_2O$ $E°= -0.38$ V (5)

$CO_2 + 8H^+ + 8e^- \rightarrow CH_4 + 2H_2O$ $E°= -0.24$ V (6)

$2H_2O + 2e^- \rightarrow H_2 + 2OH^-$ $E°= -0.41$ V (7)

$CS = [CO_2 \text{ reduction products}] / [H_2]$ (8)

$\text{Faradaic efficiency} = Q_{CO_2 \text{ reduction products}} / Q_{\text{total products}}$ (9)

The Saveant group has summarized a diagram representing most CO_2 reduction products (not including multi carbon products starting from oxalate) and their related standard potential reaction to pH in aqueous solution (Figure 1.2).[11] The diagram also indicates the involvement of not only electrons, but also protons in CO_2 reduction. The reaction is energetically more favorable with protons involved.

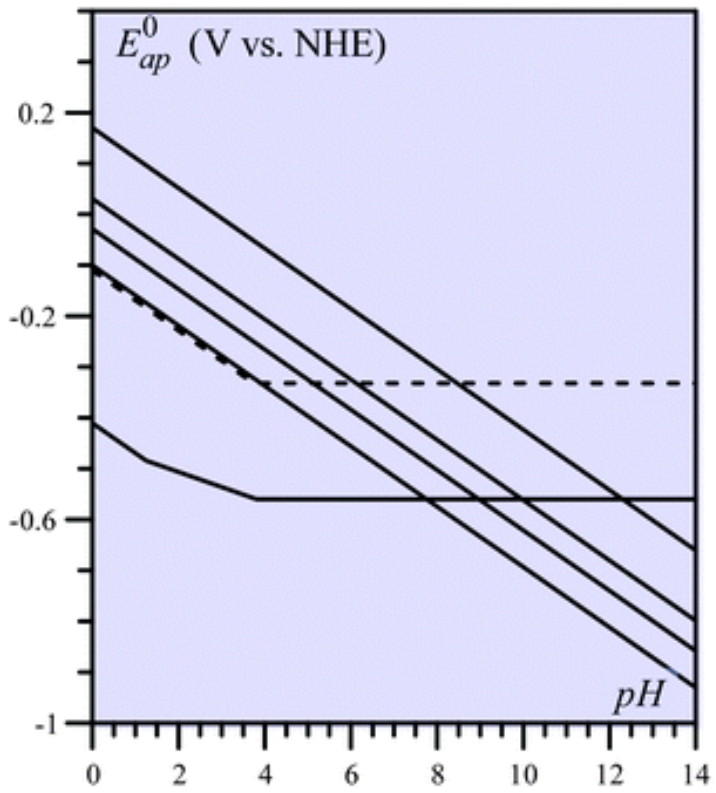

Figure 1.2. Variation of the apparent standard potential, E^0_{ap}, with pH (Pourbaix diagrams) for the reductive conversion of CO_2 into the following products. In the order of decreasing values of E^0_{ap} at pH = 0: CH_4, CH_3OH, CH_2O, CO (full line), HCO_2H, HCO_2^- (dashed line), $C_2O_4H_2$, $C_2O_4H^-$, C_2O_4. The slopes are RTln10/F with the exception of the horizontal lines and of the formation of $C_2O_4H^-$ (RTln10/2F)[11]. Adapted with permission from reference 11

However, most of the above multi-electron reactions still have to go through the single-electron process to form a radical anion intermediate[8], which requires large reorganization energy and becomes a limiting step of CO_2 reduction. The activation

energy can be reduced and the stability of the intermediate can be enhanced by catalysts[12]. Nevertheless, the mechanisms of these processes remain unclear and need clarification.

1.2. Brief review of current CO_2 reduction catalysis

Two strategies of catalysis are studied; the first is using a (multiple-functioned) single catalyst, which reduces CO_2 to formic acid, formaldehyde and methanol or methane, successively. For example, the Bocarsly group used pyridine as a single catalyst to convert CO_2 to methanol.[13] The second strategy applies a panel of catalysts, in which different catalysts contribute to separate steps of reduction. The scheme of the panel catalysts is shown in Figure 1.3,[14] in which different catalysts are specialized to catalyze the reduction of CO_2 to formic acid or formate, formic acid to formaldehyde, and formaldehyde to methanol, respectively. Enzymes are often used to promote the cascade reaction, including formate dehydrogenase, formyl dehydrogenase and alcohol dehydrogenase. For example, Obert and Dave reported an enzymatically coupled sequential reduction of carbon dioxide to methanol by using a series of reactions catalyzed by these dehydrogenases. [15]

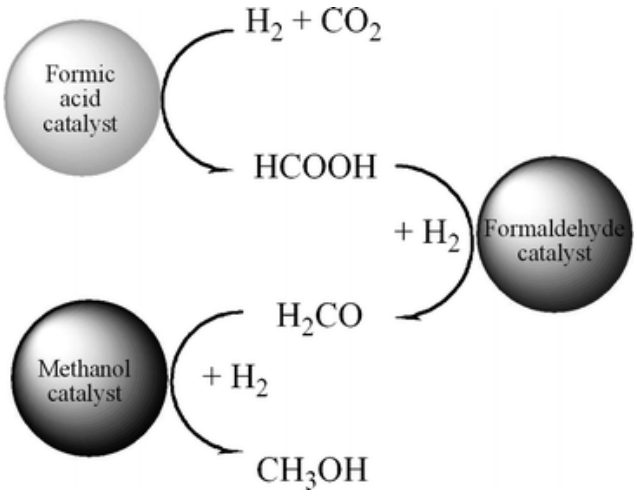

Figure 1.3. Proposed path for the tandem catalytic reduction of CO_2 to methanol. A series of three catalysts that each contributes to the overall reduction of CO_2 to methanol in optimized single steps. Adapted with permission from reference 14

1.2.1. Electrochemical CO_2 reduction

1.2.1.1. Electrodes

CO_2 can be reduced directly on the surface of electrodes to various products.

Although carbon and boron have also been reported as electrodes for CO_2 reduction, most of those electrodes being studied are metal electrodes. There are four groups of simple metal electrodes which are used for CO_2 reduction depending on the type of products, [16] as shown in Figure 1.4.[16a] The first group contains metallic copper (Cu) only, which shows great activity and selectivity in the electrochemical conversion of CO_2 to hydrocarbons. Au, Ag and Zn belong to the second group, which reduces CO_2 to CO as the main product. The third group consists of Pb, Hg, In, Sn, Cd and Tl, which yield

formate as the major product. The fourth group includes Ni, Fe, Pt, Ti and Ga, on which hydrogen evolution dominates and CO_2 reduction barely occurs without the presence of other homogeneous catalysts. Moreover, CO is reported to adsorb strongly on the metal surface in the fourth group, and in the process poisons the electrodes and prevents further CO_2 reduction.

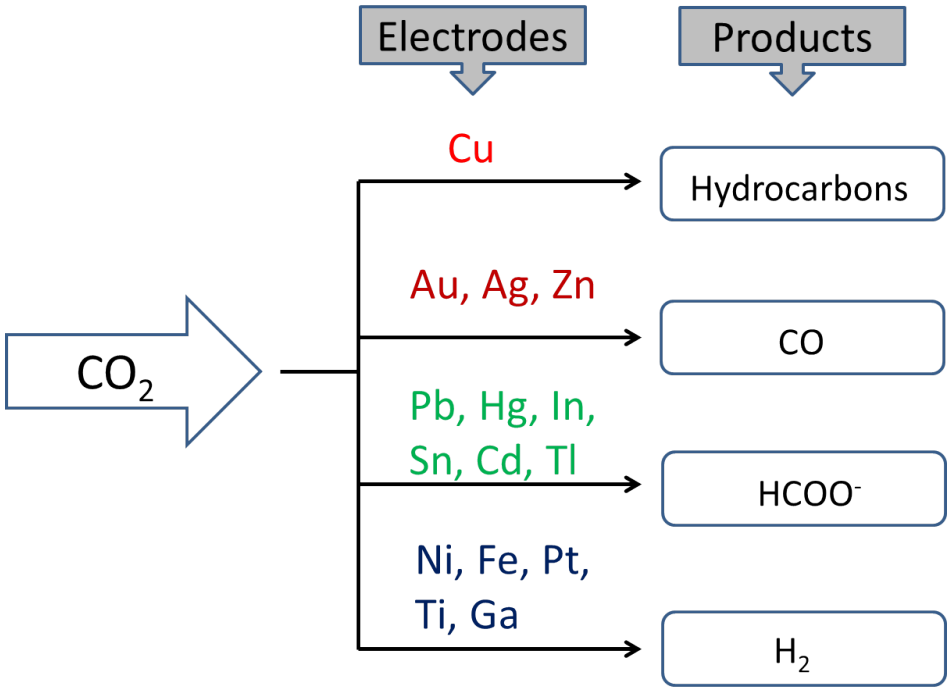

Figure 1.4. Electrode materials and reaction products of CO_2 reduction.

Adapted from Ref. 16a

The electrodes mentioned above are all amorphous structure electrodes. Similar to hydrogen evolution, the surface morphology of electrodes has great impact on the activity and selectivity of electrochemical CO_2 reduction. [17] Single crystal studies also show that different facets show different activity and selectivity towards the electrocatalytic CO_2 reduction. For example, on Cu(100) faces, C_2H_4 is the dominant product, while Cu(111) face enhances the yield of CH_4.[18] The Cu(110) faces display an enhanced selectivity towards alcohol and condensed phase C_2 and C_3 products.

Cu electrodes perform best among all the metal electrodes mentioned above in terms of activity and selectivity towards electrochemical CO_2 reduction. However, even Cu suffers from high overpotential and low current density. In aqueous solution, CO_2 reduction is coupled with water oxidation, which would increase the overpotential even more. To circumvent this problem, scientists have been trying various strategies, such as modification of electrode surfaces,[19] application of different electrolytes (molten, solid-oxide[20] or water-free ionic liquid[21] electrolytes), photo-irradiation[22] and biological microorganisms[23].

1.2.1.2. Molecular electrocatalysts

As mentioned earlier, direct reduction of CO_2 on an electrode surface usually has large overpotential and thus displays low conversion efficiency. Electrocatalysts can not only participate in the electron transfer process but also assist the related chemical reaction speed. An ideal electrocatalyst also needs to show compatible redox potential with the related chemical reaction. A large amount of research has been conducted in this field

and the majority of electrocatalysts for CO_2 reduction are molecular catalysts containing metal center(s) and appropriate ligands. Thus, the redox potential of the catalysts can be tuned via changes in metal centers and ligands. Kubiak et al. classified those metal electrocatalysts into three groups based on the ligand type, including metal catalysts with macrocyclic ligands, metal catalysts with bipyridine ligands and metal catalysts with phosphine ligands.[14] He also concluded the best strategy for developing efficient CO_2 catalysts is the combination of proton coupled multi electron transfer and appropriate catalytic sites which are capable of directing nuclear configuration of reactants to favorable product formation.

The Luca group has summarized recent state-of-art molecular electrocatalysts for CO_2 reduction, shown in Table 1.1.[24]

Table 1.1. Selected molecular catalysts for the electroctalytic reduction of CO_2, adapted from Ref. 24

	Catalyst	Potential	Conditions	Products
1[25]	$[Co^{III}N_4H(Br)_2]^{+a}$	−1.88 V vs Fc/Fc^+	20% H_2O/MeCN	CO, H_2
2[26]	$Mn(bpy\text{-}Bu)(CO)_3Br^b$	−2.2 V vs SCE	1.4 M CF_3CH_2OH/MeCN	CO
3[27]	$Re(bpy)(CO)_3Br^b$	−1.49 V vs SCE	9:1 DMF c/H_2O	CO

4[28]	$[Ni(cyclam)]^{2+}$[d]	−1 V vs NHE	0.1 M KNO_3 pH 4.1	CO
5[29]	$[Co^{I}L]^{+}$[e]	−1.34 V vs SCE	CH_3CN[f]	CO and H_2
6[30]	$[Ru(bpy)_2(CO)_2]^{2+}$[b]	−1.5 V vs SCE	DMF/H_2O 1/1	$HCOO^-$ and CO
7[31]	TPPFeCl, [g] FeTDHPPCl, [h] FeTDMPPCl[i]	−1.7 V vs SCE	DMF 0.1 M n-Bu_4NPF_6, H_2O	CO, $HCOO^-$
8[32]	CoTPP[c]	−1.9 V	Butyronitrile, n-Pr_4NClO_4	CO, $HCOO^-$
9[33]	$[(\eta^5\text{-}Me_5C_5)M(bpy)\ Cl]$ M = Ir, Rh	−1.6 V	CH_3CN, 0.1 M Bu_4NClO_4, 20% H_2O	$HCOO^-$ H_2, very little CO
10[34]	$[Pd_2(CH_3CN)_2(eHTP)](BF_4)_2$[j]	−1.3 V	DMF 0.1 M n-Bu_4NBF_4, HBF_4	CO
11[35]	[Pd(triphosphine) $(CH_3CN)](BF_4)_2$	−1.4 V	DMF 0.1 M n-Bu_4NBF_4, HBF_4	CO, H_2

[a] N_4H = 2,12-dimethyl-3,7,11,17-tetraazabicyclo-[11.3.1]-heptadeca-1(7),2,11,13,15-pentaene.

[b] Bpy: 2,2'- bipyridine.

[c] DMF: N,N'-dimethylformamide.

[d] Cyclam: 1,4,8,11-tetraazatetracyclodecane.

[e] L: 5,7,7,12,14,14-hexamethyl-1,4,8,11-tetraazacyclotetradeca-4,11-diene.

[f] pulse radiolysis experiment.

[g] TPP: tetraphenylporphyrin.

[h] TDHPP: 5,10,15,20-tetrakis(2',6'-dihydroxyphenyl)-porphyrin.

[i] TDMPP: 5,10,15,20-tetrakis(2',6'-dimethoxyphenyl)-porphyrin.

[j] eHTP: $[(Et_2PCH_2CH_2)_2PCH_2P(CH_2CH_2PEt_2)_2]$.

As shown in Table 1, it remains challenging for CO_2 reduction to compete with hydrogen evolution and H_2 often comes together as undesired products in this case. In addition, the CO_2 reduction products are $HCOO^-$ and CO, which is 2 e^- process.

Besides metal catalysts, there are also reports on organic molecules working as mediator and catalysts for CO_2 reduction, [36] such as tetraalkylammonium salts and ionic liquids as mediators, aromatic nitriles and esters as catalysts, and pyridinium derivatives. The last one will be the focus of discussion in the next section (1.3.).

1.2.2. Photochemical CO_2 reduction

As aforementioned, the ideal route of utilizing CO_2 as a feedstock is via renewable energy sources such as solar energy, thus lots of research has been done in this field. The commercially available catalyst is TiO_2-P25 because of its reproducibility. So far, compared to water splitting, there is no apparent promising CO_2 reduction photocatalyst, with low quantum yield and turnover frequency. The majority of the photocatalysts are TiO_2 based, such as systems supported by isolated centers in zeolite matrices[37] or semiconductors[38], systems with noble metals as co-catalysts[39], systems promoted by Cu[40], etc. The molecular catalysts for photochemical reduction of CO_2 are usually Re or Ru based. Bocarsly has a comprehensive review on photocatalysts and photoelectrodes for photo-driven heterogeneous CO_2 reduction.[41]

However, the TiO_2 based system has an obvious disadvantage of not being photo-responsive to visible light.[3] Thus a great amount of research has been focused on synthesizing and developing CO_2 reduction photocatalysts and systems with visible light activity. One strategy is to utilize multi-junction cells which have matching energy level, stability under illumination, and the capability of capturing the majority of the solar spectrum, overcoming the Shockley-Queiesser limit as well. [41] Organic semiconductors have also attracted some attention due to their mutability, which enables the possibility of tuning the electronics and binding relevant components, although they are much less efficient than silicon.[42]

1.3. Discussion and debate of Bocarsly work

The majority of molecular catalysts for CO_2 reduction contain a metal center. Despite this, the Bocarsly group reported pyridinium as a novel homogeneous catalyst for reducing CO_2 to methanol at a low overpotential, achieving a methanol faradaic efficiency of up to 30% at a hydrogenated Pd electrode.[43] They also reported using homogeneous pyridinium ion catalyst to selectively convert CO_2 to methanol at a p-GaP semiconductor electrode, driving the reaction with light energy at underpotential to yield faradaic efficiencies near 100%.[22a] Later, they proposed a detailed mechanism (Figure 1.5) postulating that pyridinium radical works as a one-electron shuttle for multi-electron reduction of CO_2 to methanol on a Pt disk electrode at a low overpotential (-0.58 V versus SCE).[13] Bocarsly proposed carbamate as an intermediate and suggested that pyridinium radical as a single catalyst can reduce multiple species including CO_2, formic acid and formaldehyde, resulting in a 6 e^- reduction from CO_2 to methanol. They conducted further studies on this system and concluded the electrocatalytic activation of CO_2 is the rate-determining step.[22b] In addition, they suggested the formation of carbamate again and two factors that may accelerate the reaction kinetics including the Lewis basicity of the pyridyl nitrogen and the ability of the electrode surface to stabilize carbon-based free radicals.

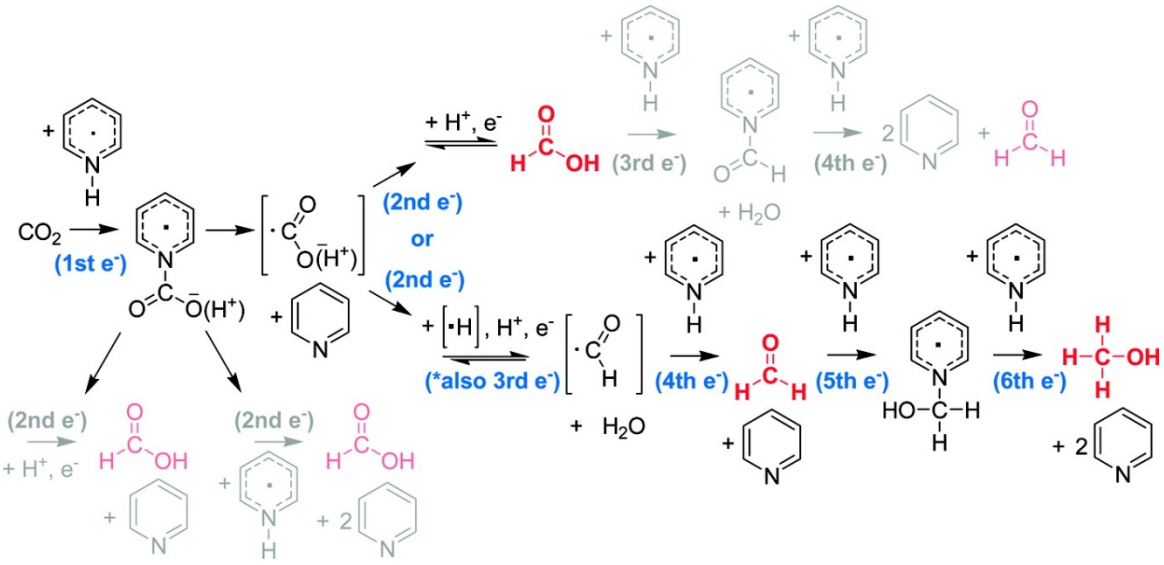

Figure 1.5. Overall Proposed Mechanism for the Pyridinium-Catalyzed Reduction of CO_2 to the Various Products of Formic Acid, Formaldehyde, and Methanol. Adapted with permission from reference 13

Much experimental and theoretical research has stemmed from Bocarsly's work and various ideas have been aroused. Pyridium as CO_2 reduction catalyst was also reported at iron pyrite[44] and Pt/C-TiO_2[45] interfaces. Costentin et al. claimed no formation of methanol and suggested that CO_2 functions similarly with pyridinium and other moderately weak acids to enhance proton reduction on platinum electrode, showing its prior conversion to carbonic acid instead of being catalytically reduced.[46] Ertem et al. found that CO_2 is reduced by H atoms bound to the platinum surface that are transferred as hydrides to CO_2 via proton-coupled hydride transfer (PCHT) mechanism activated by pyridinium, which plays the role of Brønsted acid and proton source.[47] The Bocarsly group has agreed with the surface hydride part of the mechanism in later experiments.[48]

Keith et al. conducted first-principles quantum chemistry computations and suggested that on GaP surfaces, pyridinium or proton reduction is energetically unfavorable, and instead, the 2 e^- reduction of the surface-bound pyridine to transient species such as dihydropyridine (DHP) should be feasible thermodynamically.[49] Their result also has some biomimetic implication because DHP shares a similar moiety with some biological redox catalysts. The Musgrave group suggested $PyCOOH^0$ as an intermediate for the homogeneous CO_2 reduction in the pyridine/p-GaP system, which displays aromatic stabilization and lowers the activation barrier.[50] Later, they proposed a proton transfer (PT)-electron transfer (ET)-PT-ET mechanism, converting Py to PyH_2, which is a great renewable organo-hydride donor due to its proclivity to regain aromaticity, mimicking the role of NADPH in the formation of C-H bond in the photosynthetic CO_2 reduction process. CO_2 reduction is then carried by a successive hydride transfer (HT) and PT from PyH_2.[51]

In addition, Boston et al. reported the photochemical CO_2 reduction to formate and methanol in a homogeneous system containing pyridine, Re or Ru photosensitizer, and ascorbic acid, without the presence of a metal electrode.[52]

To summarize, even though the mechanism of the pyrdinium/CO_2 system remains unclear, hydride transfer and aromatization are highly suggested factors.

1.4. The role of pterin in biologic catalysis as C1 carrier

Despite the rising amount of research on CO_2 reduction, the catalysts at present are all moderate. Scientists have also investigated the way nature does it, which is photosynthesis, and other biological regimes for new ideas.

Pterins are natural cofactor of various enzymes, functioning as redox mediator and C1 carrier between several oxidation states of a carbon-containing organic fragment. In biological systems, the pyrazine ring is fully reduced (H_4PTE) and the N5 of pyrazine is the site which carries C1 substituents. Generally, pterin, as a 2 e^- reductant, transfers electrons as hydrides.[53] A good example is the methanopterin (MPT), which is a cofactor of methanogenesis in archaea. Figure 1.6 shows the structure and partial structures of MPT's biologically active form H_4MPT. [54] The C1 substituent is first loaded at N5 of reduced MPT as a formyl group (5-HCO-H_4MPT), and then converted to a cyclic methylene intermediate (CH_2-H_4MPT) and finally reduced to a methyl group (5-CH_3-H_4MPT) in sequence. MPT has been proven as the only C1 carrier in critical steps of this pathway, without other enzymes present, except for the initial steps. [54-55] Methanol or methane is formed as the final product in H_4MPT sequence reaction, of which the net pathway shown in eqn. (10), and it gives some insights to the design of CO_2 reduction catalysts.

$$CO_2 + 4H_2 \rightarrow CH_4 + 2H_2O \qquad (10)$$

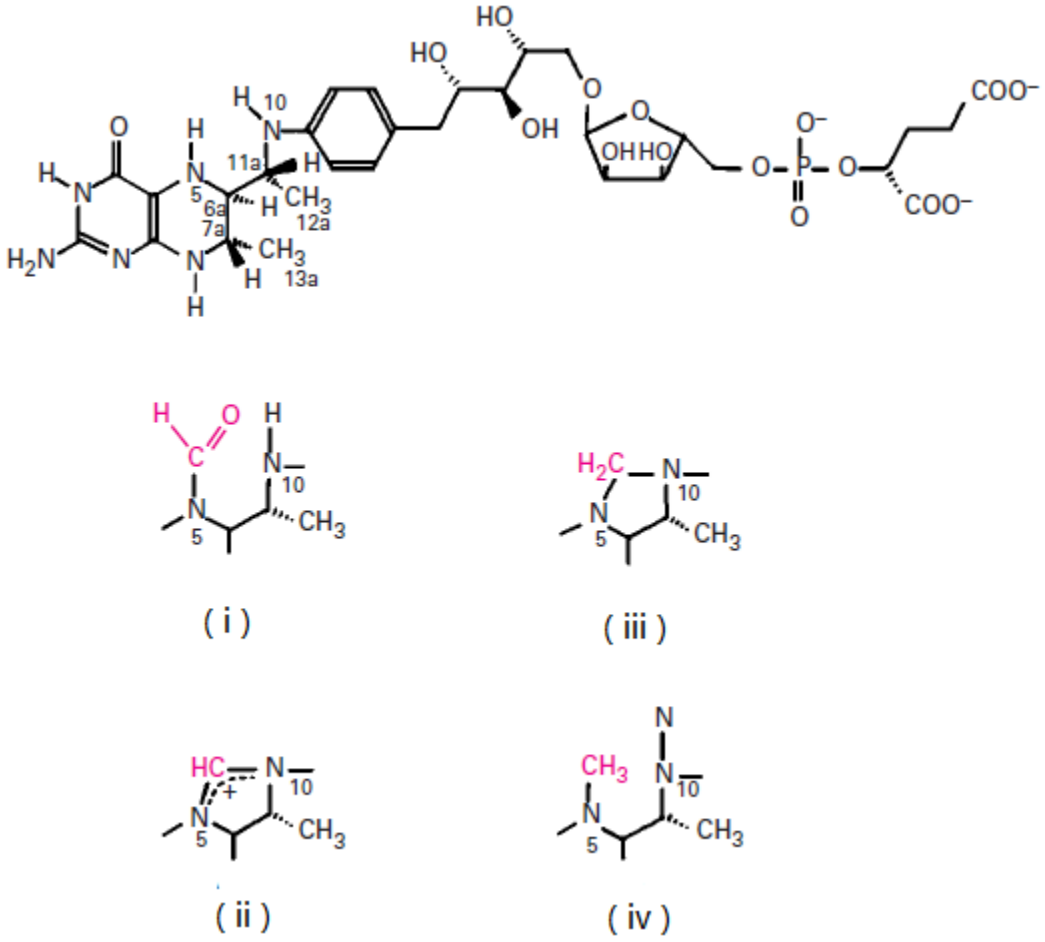

Figure 1.6. Structures of H_4MPT and partial structures of H_4MPT derivatives: (i) 5-HCO-H_4MPT; (ii) CH^+-H_4MPT;(iii) CH_2-H_4MPT; (iv) 5-CH_3-H_4MPT, Adapted from Ref. 54

Besides, the electrochemistry of pterin has long been studied. The active form of pterin is its reduced form as aforementioned, which can be produced electrochemically. Dryhurst et al. has shown a comprehensive route, shown in figure 1.7.[56] In the diagram, pterin displays two-electron redox chemistry.

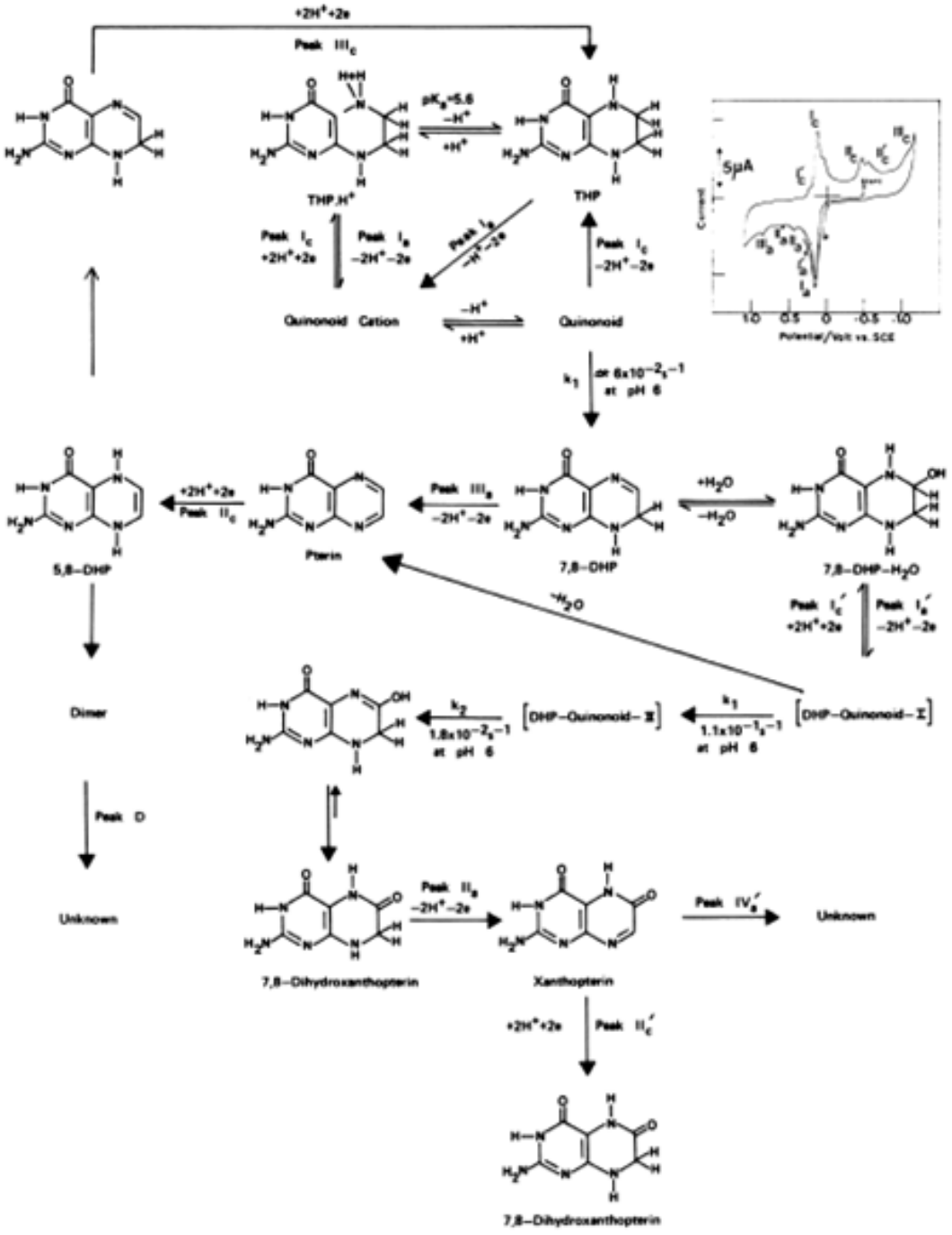

Figure 1.7. Redox chemistry of pterin, 7,8-DHP, and THP in aqueous solution. Adapted with permission from reference 56

All those characteristics of pterin mentioned above makes it a promising candidate towards CO_2 reduction catalysis. We picked 6,7-dimethyl-4-hydroxy-2-mercaptopter 6,7-dimethyl-4-hydroxy-2-mercaptopteridine (PTE) for study for multiple reasons. First it is commercially available. Second, it is chemically simple and easier to handle than biological pterins such as MPT. Third, the SH function is a convenient group for attaching the catalyst to an electrode or quantum dot surface.

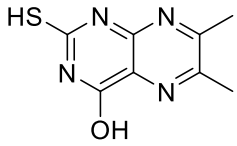

Figure 1.8. Structure of 6,7-dimethyl-4-hydroxy-2-mercaptopter 6,7-dimethyl-4-hydroxy-2-mercaptopteridine (PTE)

References

1. Hansen, J.; Sato, M.; Russell, G.; Kharecha, P., Climate sensitivity, sea level and atmospheric carbon dioxide. *Philos T R Soc A* **2013,** *371* (2001).

2. Hansen, J.; Sato, M.; Ruedy, R.; Nazarenko, L.; Lacis, A.; Schmidt, G. A.; Russell, G.; Aleinov, I.; Bauer, M.; Bauer, S.; Bell, N.; Cairns, B.; Canuto, V.; Chandler,

M.; Cheng, Y.; Del Genio, A.; Faluvegi, G.; Fleming, E.; Friend, A.; Hall, T.; Jackman, C.; Kelley, M.; Kiang, N.; Koch, D.; Lean, J.; Lerner, J.; Lo, K.; Menon, S.; Miller, R.; Minnis, P.; Novakov, T.; Oinas, V.; Perlwitz, J.; Perlwitz, J.; Rind, D.; Romanou, A.; Shindell, D.; Stone, P.; Sun, S.; Tausnev, N.; Thresher, D.; Wielicki, B.; Wong, T.; Yao, M.; Zhang, S., Efficacy of climate forcings. *J Geophys Res-Atmos* **2005,** *110* (D18).

3. Kondratenko, E. V.; Mul, G.; Baltrusaitis, J.; Larrazabal, G. O.; Perez-Ramirez, J., Status and perspectives of CO2 conversion into fuels and chemicals by catalytic, photocatalytic and electrocatalytic processes. *Energy & Environmental Science* **2013,** *6* (11), 3112-3135.

4. (a) Cokoja, M.; Bruckmeier, C.; Rieger, B.; Herrmann, W. A.; Kuhn, F. E., Transformation of carbon dioxide with homogeneous transition-metal catalysts: a molecular solution to a global challenge? *Angew Chem Int Ed Engl* **2011,** *50* (37), 8510-37; (b) Aresta, M., *Carbon dioxide as chemical feedstock*. Wiley-VCH: Weinheim, 2010; p xix, 394 p.

5. Graves, C.; Ebbesen, S. D.; Mogensen, M.; Lackner, K. S., Sustainable hydrocarbon fuels by recycling CO2 and H2O with renewable or nuclear energy. *Renewable and Sustainable Energy Reviews* **2011,** *15* (1), 1-23.

6. (a) Creutz, C. F., E. *Carbon Management: Implications for R&D in the Chemical Sciences and Technology(A Workshop Report to the Chemical Sciences Roundtable)*; National Academies Press (US): Washington (DC), 2001; (b) Jitaru, M., Electrochemical Carbon Dioxide Reduction-Fundamental and Applied Topics. *J. Univ.Chem. Tech. Metall* **2007,** *42* (4), 333-344.

7. Bard, A. J.; Faulkner, L. R., Electrochemical Methods: Fundamentals and Applications. 2nd ed.; John Wiley & Sons: New York, 2000.

8. Fujita, E.; Brunschiwig, B. S., Catalysis of Electron Transfer, Heterogeneous Systems, Gas Phase Systems. In Electron Transfer in Chemistry. Balzani, V., Ed. Wiley-VCH: Weinheim, Germany, 2001; pp. 88-126.

9. (a) Halmann, M. M.; Steinberg, M., Greenhouse Gas Carbon Dioxide Mitigation Science and Technology. Lewis Publishers: 1999; (b) Sutin;, N.; Creutz;, C.; Fujita, E., Photo-Induced Generation of Dihydrogen and Reduction of Carbon Dioxide Using Transition Metal Complexes. *Comments Inorg. Chem.* **1997,** *19* (2), 67-92; (c) Schwarz, H. A.; Dodson, R. W., Reduction Potentials of Co2- and the Alcohol Radicals. *J Phys Chem-Us* **1989,** *93* (1), 409-414.

10. Morris, A. J.; Meyer, G. J.; Fujita, E., Molecular Approaches to the Photocatalytic Reduction of Carbon Dioxide for Solar Fuels. *Accounts Chem Res* **2009,** *42* (12), 1983-1994.

11. Costentin, C.; Robert, M.; Saveant, J. M., Catalysis of the electrochemical reduction of carbon dioxide. *Chemical Society reviews* **2013,** *42* (6), 2423-2436.

12. Wheatley, M. G.; McDonagh, A. M.; Brungs, M. P.; Chaplin, R. P.; Sizgek, E., A study of reverse bias in a dye sensitised photoelectrochemical device. *Sol Energ Mat Sol C* **2003,** *76* (2), 175-181.

13. Cole, E. B.; Lakkaraju, P. S.; Rampulla, D. M.; Morris, A. J.; Abelev, E.; Bocarsly, A. B., Using a One-Electron Shuttle for the Multielectron Reduction of CO_2 to Methanol: Kinetic, Mechanistic, and Structural Insights. *J Am Chem Soc* **2010,** *132* (33), 11539-11551.

14. Benson, E. E.; Kubiak, C. P.; Sathrum, A. J.; Smieja, J. M., Electrocatalytic and homogeneous approaches to conversion of CO_2 to liquid fuels. *Chemical Society reviews* **2009,** *38* (1), 89-99.

15. Obert, R.; Dave, B. C., Enzymatic Conversion of Carbon Dioxide to Methanol: Enhanced Methanol Production in Silica Sol−Gel Matrices. *J Am Chem Soc* **1999,** *121* (51), 12192-12193.

16. (a) Hori, Y., CO_2-reduction, catalyzed by metal electrodes. In *Handbook of Fuel Cells*, John Wiley & Sons, Ltd: 2010; (b) Hori, Y.; Murata, A.; Takahashi, R., Formation of hydrocarbons in the electrochemical reduction of carbon dioxide at a copper electrode in aqueous solution. *Journal of the Chemical Society, Faraday Transactions 1: Physical Chemistry in Condensed Phases* **1989,** *85* (8), 2309-2326; (c) Hori, Y.; Wakebe, H.; Tsukamoto, T.; Koga, O., Electrocatalytic process of CO selectivity in electrochemical reduction of CO_2 at metal electrodes in aqueous media. *Electrochim Acta* **1994,** *39* (11), 1833-1839.

17. Cook, R. L.; MacDuff, R. C.; Sammells, A. F., On the Electrochemical Reduction of Carbon Dioxide at In Situ Electrodeposited Copper. *J Electrochem Soc* **1988,** *135* (6), 1320-1326.

18. Hori, Y.; Takahashi, I.; Koga, O.; Hoshi, N., Electrochemical reduction of carbon dioxide at various series of copper single crystal electrodes. *Journal of Molecular Catalysis A: Chemical* **2003,** *199* (1–2), 39-47.

19. (a) Gonçalves, M. R.; Gomes, A.; Condeço, J.; Fernandes, R.; Pardal, T.; Sequeira, C. A. C.; Branco, J. B., Selective electrochemical conversion of CO2 to C2 hydrocarbons. *Energy Conversion and Management* **2010,** *51* (1), 30-32; (b) Le, M.; Ren, M.; Zhang, Z.;

Sprunger, P. T.; Kurtz, R. L.; Flake, J. C., Electrochemical Reduction of CO_2 to CH_3OH at Copper Oxide Surfaces. *J Electrochem Soc* **2011,** *158* (5), E45-E49; (c) Li, C. W.; Kanan, M. W., CO_2 Reduction at Low Overpotential on Cu Electrodes Resulting from the Reduction of Thick Cu_2O Films. *J Am Chem Soc* **2012,** *134* (17), 7231-7234; (d) Chen, Y.; Kanan, M. W., Tin Oxide Dependence of the CO2 Reduction Efficiency on Tin Electrodes and Enhanced Activity for Tin/Tin Oxide Thin-Film Catalysts. *J Am Chem Soc* **2012,** *134* (4), 1986-1989; (e) Chen, Z.; Kang, P.; Zhang, M.-T.; Stoner, B. R.; Meyer, T. J., Cu(II)/Cu(0) electrocatalyzed CO_2 and H_2O splitting. *Energy & Environmental Science* **2013,** *6* (3), 813-817.

20. (a) Hu, B.; Stancovski, V.; Morton, M.; Suib, S. L., Enhanced electrocatalytic reduction of CO_2/H_2O to paraformaldehyde at Pt/metal oxide interfaces. *Applied Catalysis A: General* **2010,** *382* (2), 277-283; (b) Xie, K.; Zhang, Y.; Meng, G.; Irvine, J. T. S., Electrochemical reduction of CO_2 in a proton conducting solid oxide electrolyser. *J Mater Chem* **2011,** *21* (1), 195-198.

21. Rosen, B. A.; Salehi-Khojin, A.; Thorson, M. R.; Zhu, W.; Whipple, D. T.; Kenis, P. J. A.; Masel, R. I., Ionic Liquid–Mediated Selective Conversion of CO_2 to CO at Low Overpotentials. *Science* **2011,** *334* (6056), 643-644.

22. (a) Barton, E. E.; Rampulla, D. M.; Bocarsly, A. B., Selective Solar-Driven Reduction of CO_2 to Methanol Using a Catalyzed p-GaP Based Photoelectrochemical Cell. *J Am Chem Soc* **2008,** *130* (20), 6342-6344; (b) Morris, A. J.; McGibbon, R. T.; Bocarsly, A. B., Electrocatalytic carbon dioxide activation: the rate-determining step of pyridinium-catalyzed CO_2 reduction. *Chemsuschem* **2011,** *4* (2), 191-6.

23. (a) Cheng, S.; Xing, D.; Call, D. F.; Logan, B. E., Direct Biological Conversion of Electrical Current into Methane by Electromethanogenesis. *Environmental Science & Technology* **2009,** *43* (10), 3953-3958; (b) Villano, M.; Aulenta, F.; Ciucci, C.; Ferri, T.; Giuliano, A.; Majone, M., Bioelectrochemical reduction of CO_2 to CH_4 via direct and indirect extracellular electron transfer by a hydrogenophilic methanogenic culture. *Bioresource Technology* **2010,** *101* (9), 3085-3090; (c) Zhao, H.; Zhang, Y.; Zhao, B.; Chang, Y.; Li, Z., Electrochemical Reduction of Carbon Dioxide in an MFC–MEC System with a Layer-by-Layer Self-Assembly Carbon Nanotube/Cobalt Phthalocyanine Modified Electrode. *Environmental Science & Technology* **2012,** *46* (9), 5198-5204; (d) Van Eerten-Jansen, M. C. A. A.; Heijne, A. T.; Buisman, C. J. N.; Hamelers, H. V. M., Microbial electrolysis cells for production of methane from CO2: long-term performance and perspectives. *International Journal of Energy Research* **2012,** *36* (6), 809-819; (e) Mogi, T.; Ishii, T.; Hashimoto, K.; Nakamura, R., Low-voltage electrochemical CO2 reduction by bacterial voltage-multiplier circuits. *Chem Commun* **2013,** *49* (38), 3967-3969.

24. Fenwick, A. Q.; Gregoire, J. M.; Luca, O. R., Electrocatalytic Reduction of Nitrogen and Carbon Dioxide to Chemical Fuels: Challenges and Opportunities for a Solar Fuel Device. *J Photoch Photobio B* **2015,** *152*, 47-57.

25. Lacy, D. C.; McCrory, C. C. L.; Peters, J. C., Studies of Cobalt-Mediated Electrocatalytic CO2 Reduction Using a Redox-Active Ligand. *Inorg Chem* **2014,** *53* (10), 4980-4988.

26. (a) Smieja, J. M.; Sampson, M. D.; Grice, K. A.; Benson, E. E.; Froehlich, J. D.; Kubiak, C. P., Manganese as a Substitute for Rhenium in CO_2 Reduction Catalysts: The

Importance of Acids. *Inorg Chem* **2013,** *52* (5), 2484-2491; (b) Bourrez, M.; Molton, F.; Chardon-Noblat, S.; Deronzier, A., [Mn(bipyridyl)$(CO)_3$Br]: An Abundant Metal Carbonyl Complex as Efficient Electrocatalyst for CO_2 Reduction. *Angewandte Chemie* **2011,** *123* (42), 10077-10080.

27. (a) Benson, E. E.; Sampson, M. D.; Grice, K. A.; Smieja, J. M.; Froehlich, J. D.; Friebel, D.; Keith, J. A.; Carter, E. A.; Nilsson, A.; Kubiak, C. P., The Electronic States of Rhenium Bipyridyl Electrocatalysts for CO_2 Reduction as Revealed by X-ray Absorption Spectroscopy and Computational Quantum Chemistry. *Angewandte Chemie International Edition* **2013,** *52* (18), 4841-4844; (b) Hawecker, J.; Lehn, J.-M.; Ziessel, R., Electrocatalytic reduction of carbon dioxide mediated by Re(bipy)$(CO)_3$Cl (bipy = 2,2[prime or minute]-bipyridine). *Journal of the Chemical Society, Chemical Communications* **1984,** (6), 328-330; (c) Sampson, M. D.; Froehlich, J. D.; Smieja, J. M.; Benson, E. E.; Sharp, I. D.; Kubiak, C. P., Direct observation of the reduction of carbon dioxide by rhenium bipyridine catalysts. *Energy & Environmental Science* **2013,** *6* (12), 3748-3755.

28. (a) Froehlich, J. D.; Kubiak, C. P., Homogeneous CO_2 Reduction by Ni(cyclam) at a Glassy Carbon Electrode. *Inorg Chem* **2012,** *51* (7), 3932-3934; (b) Beley, M.; Collin, J. P.; Ruppert, R.; Sauvage, J. P., Electrocatalytic reduction of carbon dioxide by nickel cyclam^{2+} in water: study of the factors affecting the efficiency and the selectivity of the process. *J Am Chem Soc* **1986,** *108* (24), 7461-7467.

29. Fisher, B. J.; Eisenberg, R., Electrocatalytic reduction of carbon dioxide by using macrocycles of nickel and cobalt. *J Am Chem Soc* **1980,** *102* (24), 7361-7363.

30. Ishida, H.; Tanaka, K.; Tanaka, T., Electrochemical CO_2 reduction catalyzed by ruthenium complexes $[Ru(bpy)_2(CO)_2]^{2+}$ and $[Ru(bpy)_2(CO)Cl]^{+}$. Effect of pH on the formation of CO and HCOO. *Organometallics* **1987,** *6* (1), 181-186.

31. Costentin, C.; Drouet, S.; Robert, M.; Savéant, J.-M., A Local Proton Source Enhances CO_2 Electroreduction to CO by a Molecular Fe Catalyst. *Science* **2012,** *338* (6103), 90-94.

32. Behar, D.; Dhanasekaran, T.; Neta, P.; Hosten, C. M.; Ejeh, D.; Hambright, P.; Fujita, E., Cobalt Porphyrin Catalyzed Reduction of CO_2. Radiation Chemical, Photochemical, and Electrochemical Studies. *The Journal of Physical Chemistry A* **1998,** *102* (17), 2870-2877.

33. Caix, C.; Chardon-Noblat, S.; Deronzier, A., Electrocatalytic reduction of CO_2 into formate with [(η5□Me5C5)M(L)Cl]+ complexes (L = 2,2′-bipyridine ligands; M □ Rh(III) and Ir(III)). *J Electroanal Chem* **1997,** *434* (1–2), 163-170.

34. Steffey, B. D.; Curtis, C. J.; DuBois, D. L., Electrochemical Reduction of CO_2 Catalyzed by a Dinuclear Palladium Complex Containing a Bridging Hexaphosphine Ligand: Evidence for Cooperativity. *Organometallics* **1995,** *14* (10), 4937-4943.

35. DuBois, D. L.; Miedaner, A.; Haltiwanger, R. C., Electrochemical reduction of carbon dioxide catalyzed by [Pd(triphosphine)(solvent)]$(BF_4)_2$ complexes: synthetic and mechanistic studies. *J Am Chem Soc* **1991,** *113* (23), 8753-8764.

36. Oh, Y.; Hu, X. L., Organic molecules as mediators and catalysts for photocatalytic and electrocatalytic CO_2 reduction. *Chemical Society reviews* **2013,** *42* (6), 2253-2261.

37. (a) Ikeue, K.; Mukai, H.; Yamashita, H.; Inagaki, S.; Matsuoka, M.; Anpo, M., Characterization and photocatalytic reduction of CO_2 with H_2O on Ti/FSM-16 synthesized by various preparation methods. *Journal of Synchrotron Radiation* **2001,** *8* (2), 640-642; (b) Ikeue, K.; Yamashita, H.; Anpo, M.; Takewaki, T., Photocatalytic Reduction of CO_2 with H_2O on Ti−β Zeolite Photocatalysts: Effect of the Hydrophobic and Hydrophilic Properties. *The Journal of Physical Chemistry B* **2001,** *105* (35), 8350-8355; (c) Hwang, J.-S.; Chang, J.-S.; Park, S.-E.; Ikeue, K.; Anpo, M., Photoreduction of Carbondioxide on Surface Functionalized Nanoporous Catalysts. *Topics in Catalysis 35* (3), 311-319.

38. (a) Sasirekha, N.; Basha, S. J. S.; Shanthi, K., Photocatalytic performance of Ru doped anatase mounted on silica for reduction of carbon dioxide. *Applied Catalysis B: Environmental* **2006,** *62* (1–2), 169-180; (b) Wang, Y.; Li, B.; Zhang, C.; Cui, L.; Kang, S.; Li, X.; Zhou, L., Ordered mesoporous CeO_2-TiO_2 composites: Highly efficient photocatalysts for the reduction of CO_2 with H_2O under simulated solar irradiation. *Applied Catalysis B: Environmental* **2013,** *130–131*, 277-284.

39. Ishitani; Osamu; Inoue, C.; Suzuki, Y.; Ibusuki, T., Photocatalytic reduction of carbon dioxide to methane and acetic acid by an aqueous suspension of metal-deposited TiO_2. *Journal of Photochemistry and Photobiology A: Chemistry* **1993,** *72* (3), 269-271.

40. (a) Dhakshinamoorthy, A.; Navalon, S.; Corma, A.; Garcia, H., Photocatalytic CO2 reduction by TiO2 and related titanium containing solids. *Energy & Environmental Science* **2012,** *5* (11), 9217-9233; (b) Li, Y.; Wang, W.-N.; Zhan, Z.; Woo, M.-H.; Wu, C.-Y.; Biswas, P., Photocatalytic reduction of CO_2 with H_2O on mesoporous silica

supported Cu/TiO2 catalysts. *Applied Catalysis B: Environmental* **2010,** *100* (1–2), 386-392.

41. White, J. L.; Baruch, M. F.; Pander, J. E.; Hu, Y.; Fortmeyer, I. C.; Park, J. E.; Zhang, T.; Liao, K.; Gu, J.; Yan, Y.; Shaw, T. W.; Abelev, E.; Bocarsly, A. B., Light-Driven Heterogeneous Reduction of Carbon Dioxide: Photocatalysts and Photoelectrodes. *Chem Rev* **2015,** *115* (23), 12888-12935.

42. (a) Green, M. A.; Emery, K.; Hishikawa, Y.; Warta, W.; Dunlop, E. D., Solar cell efficiency tables (Version 45). *Progress in Photovoltaics: Research and Applications* **2015,** *23* (1), 1-9; (b) Li, C.; Liu, M.; Pschirer, N. G.; Baumgarten, M.; Müllen, K., Polyphenylene-Based Materials for Organic Photovoltaics. *Chem Rev* **2010,** *110* (11), 6817-6855.

43. Seshadri, G.; Lin, C.; Bocarsly, A. B., A new homogeneous electrocatalyst for the reduction of carbon dioxide to methanol at low overpotential. *J Electroanal Chem* **1994,** *372* (1–2), 145-150.

44. Bocarsly, A. B.; Gibson, Q. D.; Morris, A. J.; L'Esperance, R. P.; Detweiler, Z. M.; Lakkaraju, P. S.; Zeitler, E. L.; Shaw, T. W., Comparative Study of Imidazole and Pyridine Catalyzed Reduction of Carbon Dioxide at Illuminated Iron Pyrite Electrodes. *Acs Catal* **2012,** *2* (8), 1684-1692.

45. de Tacconi, N. R.; Chanmanee, W.; Dennis, B. H.; MacDonnell, F. M.; Boston, D. J.; Rajeshwar, K., Electrocatalytic Reduction of Carbon Dioxide Using Pt/C-TiO_2 Nanocomposite Cathode. *Electrochemical and Solid-State Letters* **2011,** *15* (1), B5-B8.

46. Costentin, C.; Canales, J. C.; Haddou, B.; Saveant, J. M., Electrochemistry of Acids on Platinum. Application to the Reduction of Carbon Dioxide in the Presence of Pyridinium Ion in Water. *J Am Chem Soc* **2013,** *135* (47), 17671-17674.

47. Ertem, M. Z.; Konezny, S. J.; Araujo, C. M.; Batista, V. S., Functional Role of Pyridinium during Aqueous Electrochemical Reduction of CO_2 on Pt(111). *J Phys Chem Lett* **2013,** *4* (5), 745-748.

48. Yan, Y.; Zeitler, E. L.; Gu, J.; Hu, Y.; Bocarsly, A. B., Electrochemistry of Aqueous Pyridinium: Exploration of a Key Aspect of Electrocatalytic Reduction of CO_2 to Methanol. *J Am Chem Soc* **2013,** *135* (38), 14020-14023.

49. Keith, J. A.; Carter, E. A., Theoretical Insights into Electrochemical CO_2 Reduction Mechanisms Catalyzed by Surface-Bound Nitrogen Heterocycles. *J Phys Chem Lett* **2013,** *4* (23), 4058-4063.

50. Lim, C. H.; Holder, A. M.; Musgrave, C. B., Mechanism of Homogeneous Reduction of CO_2 by Pyridine: Proton Relay in Aqueous Solvent and Aromatic Stabilization. *J Am Chem Soc* **2013,** *135* (1), 142-154.

51. (a) Lim, C. H.; Holder, A. M.; Hynes, J. T.; Musgrave, C. B., Reduction of CO_2 to Methanol Catalyzed by a Biomimetic Organo-Hydride Produced from Pyridine. *J Am Chem Soc* **2014,** *136* (45), 16081-16095; (b) Lim, C. H.; Holder, A. M.; Hynes, J. T.; Musgrave, C. B., Catalytic Reduction of CO_2 by Renewable Organohydrides. *J Phys Chem Lett* **2015,** *6* (24), 5078-5092.

52. (a) Boston, D. J.; Pachon, Y. M. F.; Lezna, R. O.; de Tacconi, N. R.; MacDonnell, F. M., Electrocatalytic and Photocatalytic Conversion of CO_2 to Methanol using Ruthenium Complexes with Internal Pyridyl Cocatalysts. *Inorg Chem* **2014,** *53* (13),

6544-6553; (b) Boston, D. J.; Xu, C. D.; Armstrong, D. W.; MacDonnell, F. M., Photochemical Reduction of Carbon Dioxide to Methanol and Formate in a Homogeneous System with Pyridinium Catalysts. *J Am Chem Soc* **2013,** *135* (44), 16252-16255.

53. Keltjens, J. T.; Vanderdrift, C., Electron-Transfer Reactions in Methanogens. *Fems Microbiol Lett* **1986,** *39* (3), 259-303.

54. Maden, B. E. H., Tetrahydrofolate and tetrahydromethanopterin compared: functionally distinct carriers in C-1 metabolism. *Biochem J* **2000,** *350*, 609-629.

55. Dimarco, A. A.; Bobik, T. A.; Wolfe, R. S., Unusual Coenzymes of Methanogenesis. *Annu Rev Biochem* **1990,** *59*, 355-394.

56. Dryhurst, G.; Raghavan, R.; Egeserpkenci, D.; Karber, L. G., Electrochemistry of Reduced Pterin Cofactors. *Advances in Chemistry Series* **1982,** (201), 457-487.

Chapter 2. CO_2 Reduction Catalyzed by Mercaptopyridine and its Derivatives Attached on Gold Film

2.1. Introduction

Carbon emission has accelerated due to anthropogenic activities, and CO_2, a potent greenhouse gas, has become a contributor to climate forcing.[1] Thus, there is a need to develop a carbon neutral energy cycle. In addition, the amount of fossil fuel, which is the essential part of the global energy requirement, is not infinite and will decrease as consumption increases, especially since the world population is growing and the life expectancy is increasing. Therefore, converting the nontoxic and abundant CO_2 to useful fuels, ideally through renewable energy, has long been a popular research topic because of the possibility to alleviate those two issues. The Bocarsly group reported that pyridinium can catalyze 6 e- reduction of CO_2 to methanol.[2] Motivated by analogy to biological enzyme cofactors, we also tested pteridine as a possible CO_2 reduction catalyst.[3]

Thiol-gold chemistry has been widely applied in the fields of materials science and engineering. [4] Systems involving thiol-gold chemistry have gained interest due to their versatile applications, such as the fabrication of molecular scale devices and nanopatterning, and the formation of biosurfaces. [5] Here we studied mercaptopyridine and mercaptopteridine, which have a thiol functional group through which they can be attached on gold films. Thus, we can obtain a monolayer of catalyst on the gold film

surface, which has a potential to be utilized in future catalytic device development. The catalyst attached on gold film showed reduction of CO_2 to formate, folmaldehyde and methanol.

2.2. Experiment section

2.2.1. Chemicals and materials

20 mM (or 10 mM) Pyridine, 4-mercaptopyridine (Spy) and 6,7-dimethyl-4-hydroxy-2-mercaptopteridine (PTE) are prepared (the catalyst was obtained from Sigma-Aldrich and used without further purification), in addition to 500 mM potassium chloride (KCl, EMD) works as supporting electrolyte. The solution is degassed by Argon for 20 min and pH is maintained the same for both solutions saturated by Ar and CO_2.

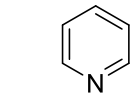

Pyridine (Py)

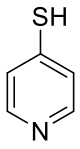

Mercaptopyridine (Spy)

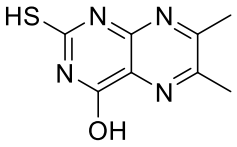

6,7-dimethyl-4-hydroxy-2-mercaptopteridine (PTE)

Figure 2.1. Structures of Py, Spy and PTE

2.2.2. Electrochemistry set-up

All electrochemical measurements are performed on a Reference 3000 Potentiostat/ Galvanostat/ZRA (Gamry Instruments). A three-neck flask is used as electrochemical cell and a platinum wire (MW-4130, BASi) and Ag/AgCl (3 M NaCl) electrode (MF-2052, BASi) are counter electrode and reference electrode, respectively. Glassy carbon (MF-2012, BASi), gold (MF-2014, BASi) and platinum (MF-2013, BASi) are all used as working electrode. Every electrode was polished with 1 μm alumina before use. The efficient surface area of gold electrode (0.1035 cm^2) and platinum electrode (0.1035 cm^2) were obtained from the oxygen desorption and hydrogen desorption peak, respectively, in 0.5 M H_2SO_4 solution. The geometric surface area (0.07069 cm^2) was used as the real surface area for glassy carbon electrode. The scan rate is 100 mV/s if not specified.

2.2.3. FTIR set-up

In-situ FTIR measurements were performed on a Smiths Detection DurasamplIR II ATR installed on a Varian 660-IR. Using a Gamry Reference 600 potentiostat the potential was scanned collecting an infrared spectrum at each potential. The sample set up involved a homemade sample compartment that consists of a well surrounding the ATR crystal allowing the platinum working electrode to be within 5 mm from the ATR crystal. The electrochemistry consists of the 1.6 mm diameter platinum disk a platinum wire anode and a silver/silver chloride reference. Labview was used to synchronize the FTIR to the potentiostat providing the ability to change the potential and collecting the 128 scans at 2 cm^{-1} resolution.

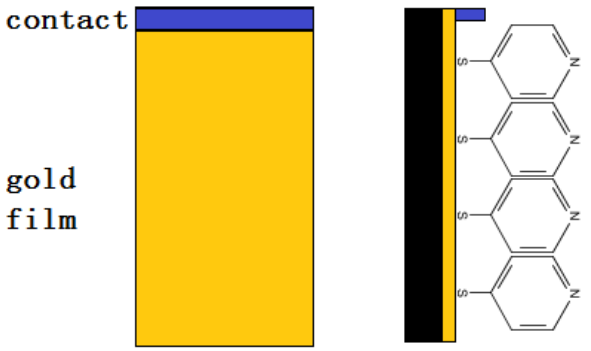

Figure 2.2. Schematic representation of Spy-Au system

2.2.4. Sample preparation and experimental process

Gold film (Ted Pella, Inc.) is cleaned in piranha solution (sulfuric acid and hydrogen peroxide in 3:1 ratio in volume) for 10 minutes and then immersed in 40 mM 4-mercaptopyridine (Spy) or 10mM 6,7-dimethyl-4-hydroxy-2-mercaptopteridine (PTE) solution (ethanol: distilled water = 3:1), which shows bright yellow color in basic environment, to attach a monolayer of Spy or PTE on it. The film is rinsed by distilled water after 4 hours immersion to wash off adsorbed acid and salts and then dried naturally in air. The gold film is connected with copper wire by superglue and Leitsilber 200 silver paste (Ted Pella, Inc.) to be the working electrode. All experiments are conducted in Deuterium oxide (D_2O, 99.9 atom% D, CIL). The starting reactant is 50 mM potassium carbonate (K_2CO_3, A.C.S reagent), in addition to 0.5 M potassium chloride (KCl, EMD) works as supporting electrolyte. The pH is adjusted to achieve pH 5.2 using Deuterium chloride solution (35 wt. % in D_2O, 99 atom % D, Aldrich). Figure 2.2 shows the schematic representation of the electrocatalyst-electrode system, where the electrocatalyst, Spy, is immobilized on gold surface because of the Au-S bond.

The solution is degassed by Argon for 20 min and then the Spy or PTE immobilized gold film is conditioned at -0.65 V (depends on the reduction potential) for 2h. The FTIR spectra are collected using Varian 660 IR Spectrometer. The sample solution in the electrochemical cell is flowed to the transmission cell by using Rabbit-HP solvent delivery system (Rainin Instrument Co. Inc.). The path length is 100 μM for measurement, which is created by Teflon spacer between two polished circular CaF_2 windows (25 mm, Koch Crystal Finishing, Inc.). All the data acquisition is achieved using LabVIEW (National Instruments) to synchronize electrochemical conditioning and FTIR data collecting automatically every 5 min.

2.2.5. Gas chromatography

At end, the product solution is analyzed by gas chromatography (GC) to verify the final products. Agilent 7890A GC is equipped with a FID detector and HP-5 column (Agilent Technologies). The inlet temperature was held at 250 °C and pressure was at 3 psi; the detector temperature was at 300 °C. The oven temperature was set to gradient heating, in which the initial temperature was 40 °C, holding for 1 min, and then increased at a rate of 10 °C/min till 120 °C.

2.3. Results and discussion

We first investigated the redox chemistry of pyridine and its derivatives on multiple electrodes in bulk solution, to obtain some information about the redox properties of these compounds. After attaching Spy and PTE directly to gold surface we used CV, FTIR and GC to monitor the reaction process of carbonate under catalyst-attached gold

electrode, and to detect the possible products. What's important is that we combine CV and FTIR together and follow the in-situ reaction.

2.3.1. Comparison of redox chemistry on different electrodes

We studied the cyclic voltammetry (CV) of all the 3 chemicals on platinum, gold and glassy carbon electrodes to characterize their redox reactions in bulk solution before the film study. Pyridine shows redox reactions on a platinum electrode (Figure 3.3a)), while it does not show an oxidation wave on a gold electrode and does not show redox on the glassy carbon electrode (Figure 3.3b)). The difference in hydrogen overpotential of the 3 electrodes might be the reason, for platinum, which has low hydrogen overpotential and thus has ample hydrogen atoms adsorbed on surface to react with surface species.

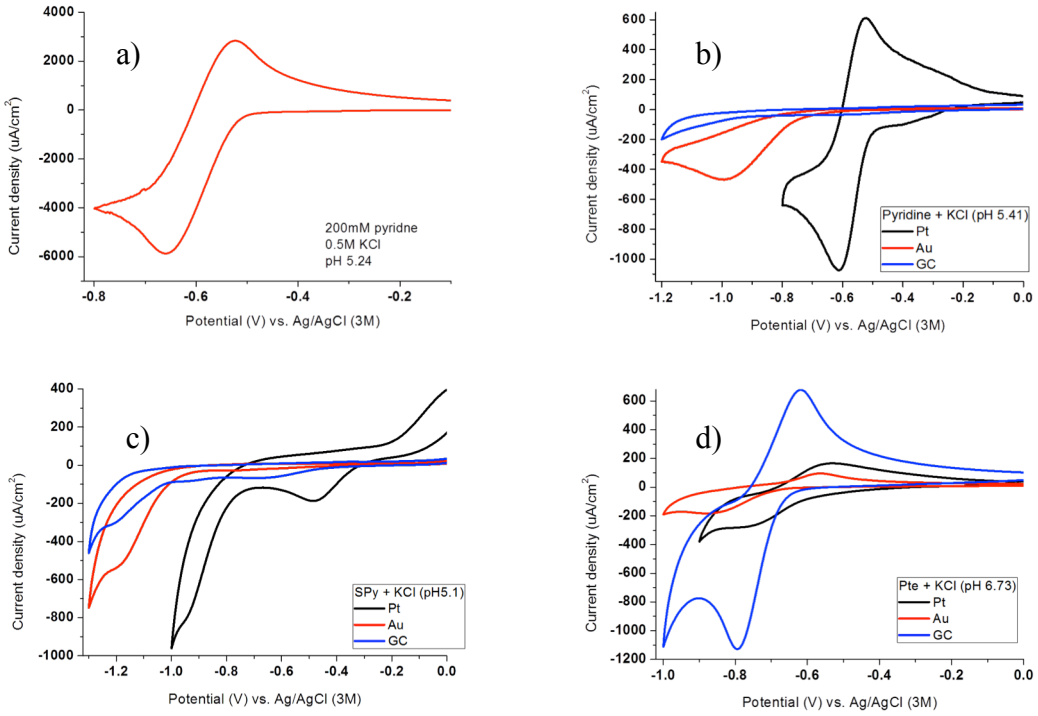

Figure 2.3. Cyclic voltammograms of a) 200 mM pyridine on Pt electrode; b) 20 mM pyridine; c) 20 mM mercaptopyridine; d) 20 mM mercaptopteridine on Pt, Au and glassy carbon electrode (0.5 M KCl as supporting electrolyte, scan rate 100 mV/s)

The lack of an oxidation wave on gold electrode means that once the pyridine is reduced it reacts with something so that the reduction is irreversible. One possible electron pathway is to water, or the reduced pyridinium radicals react with each other and therefore no oxidation of the radical occurred. A similar situation occurred with the mercaptopyridine electrochemistry on all of the three electrodes, without an observed oxidation wave on any of them. If the electron can transfer to CO_2 more efficiently than any of the unproductive pathways, it can still work as a catalyst for CO_2 reduction. In the

case of mercaptopteridine, it shows redox chemistry on all of the three electrodes, which indicates that it has the potential to be a good catalyst since it is readily reduced on all 3 electrodes and since it is reversible.

2.3.2. Studies of mercaptopyridine as a catalyst attached on gold films

To make a more efficient electron transfer between the electrocatalyst and electrode, we decided to attach the electrocatalyst, (Spy) directly to the gold electrode. By attachment to the electrode, the overpotential is expected to be reduced compared with bulk catalysis, resulting from the covalent bond formed between the electrode and catalyst. In the case of platinum, the hydrogen surface adsorption reduces the effective overpotential. The overall CO_2 reduction process should be more efficient, because multiple reduction steps are possible without requiring diffusion of the catalyst to the electrode surface. Another advantage to films is the possibility to build up multiple-component systems, for example, the introduction of quantum dots as a layer between the electrode and the catalyst.

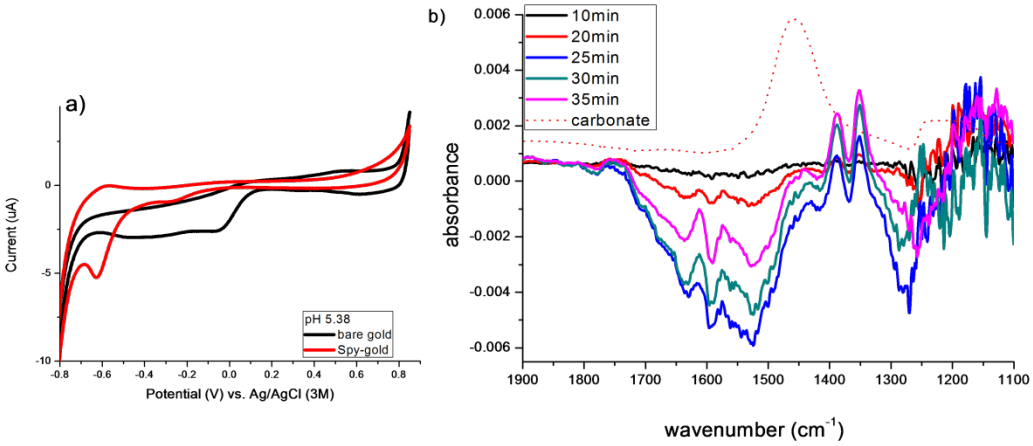

Figure 2.4. a) Cyclic voltammograms of Spy-gold and bare gold in phosphate buffer solution at pH 5.38; b) FTIR during conditioning the Spy-gold at different time

It is still necessary to investigate the catalyst-attached electrode system before introducing new components. Figure 2.4a) shows cyclic voltammograms (CVs) for bare gold and Spy attached gold in phosphate buffer solutions, which indicates the main reduction peak of attached Spy is at -0.6V at pH 5.45. CVs and FTIR spectra were collected to better compare the catalysis through pyridine bulk solution and Spy-attached gold. The Spy attached gold film is conditioned at -0.65V, which is the correct reduction potential of mercaptopyridine at pH 5.28 according the previously taken CV, where it is easier to form the proposed pyridinium radical-CO_2 intermediate through the reduced form of Spy. Figure 2.4b) shows the change of FTIR with time during conditioning. The main peaks are growing with time in the first 35 min, which further proves these peaks are due the forming of products. At the same time, the peaks of 1550 and 1250 cm^{-1} are assigned to carbonate (slightly different with the FTIR of carbonate shown in dash line

because of different pH) which show a negative pattern and represent the consumption/ disappearance of the starting reactant (carbonate).

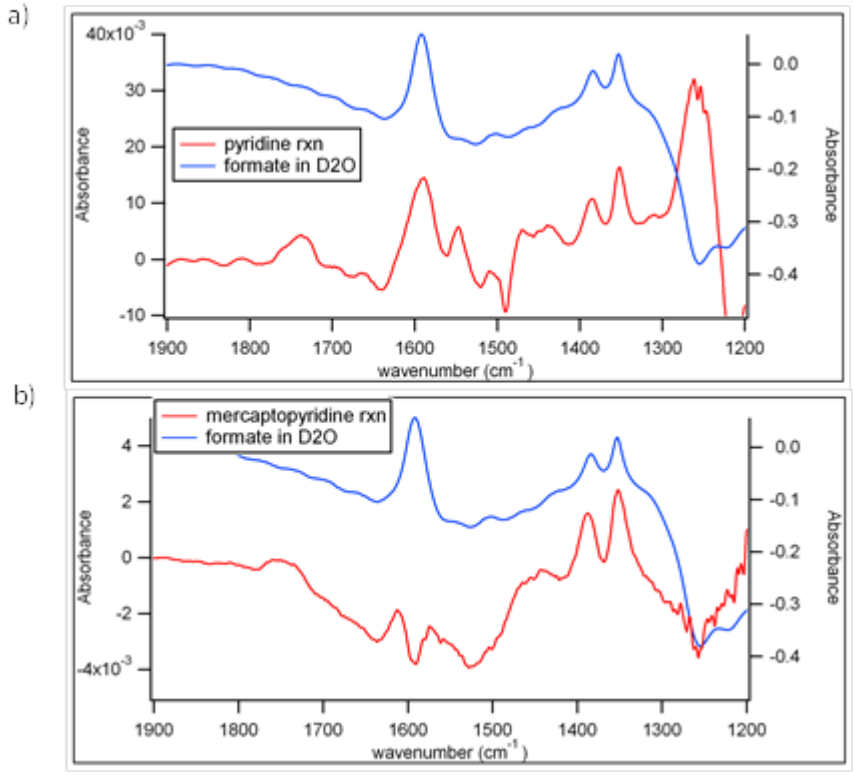

Figure 2.5. FTIR of a) pyridine bulk solution system at gold electrode and b) Spy-attached gold film during conditioning compared with formate spectrum (D_2O as solvent)

The bulk pyridine reaction was compared with the Spy-Au film under the same conditions (conditioning at -0.65 V, which is the correct the reduction potential of mercaptopyridine at pH 5.28 according the previously taken CV, where it is easier to form the proposed pyridinium radical-CO_2 intermediate through the reduced form of Spy).

In the in situ FTIR in Figure 2.5, several peaks, mainly at 1350, 1385, 1440, 1450, 1550, 1600 and 1750 cm^{-1}, are observed. Compared with the FTIR spectrum of formate in D_2O, the peaks of 1350, 1385 and 1600 cm^{-1} can be ascribed to the formation of formate. The peak around 1750 cm^{-1} suggests the formation of formic acid. Further work needs to be done to assign other peaks. However, the conclusion can be made that multiple products in addition to formate were formed during the conditioning.

2.3.3. Studies of mercaptopteridine as a catalyst attached on gold films

The pyridinium catalysis process is a nucleophilic addition-elimination reaction with the amine as the active site. In comparison, 6,7-dimethyl-4-hydroxy-2-mercaptopteridine (PTE) has the pterin ring structure, which is closer to the structure of biological cofactors and displays hydricity and aromaticity. In addition, it is easier to make the 2 e- reduced species that can do hydride transfer. Thus, PTE should exhibit more efficient CO_2 reduction. The double-ring structure also makes it possible to work as a two-electron shuttle in aqueous solution assisted by proton transfer. In addition, PTE shows redox reactions on all of the three different electrodes tested as observed in figure 3d). Figure 2.6 shows the CVs and FTIR data of the PTE attached film in 50 mM carbonate solution. PTE-attached Au film shows similar redox chemistry but different FTIR spectra with Spy-attached one, which indicates we might get different products in this case. Possible explanation for this is that, as discussed in chapter 1, the pyridine system probably involves surface hydride transfer, while the PTE works by direct hydride transfer, which may lead to different chemistry.

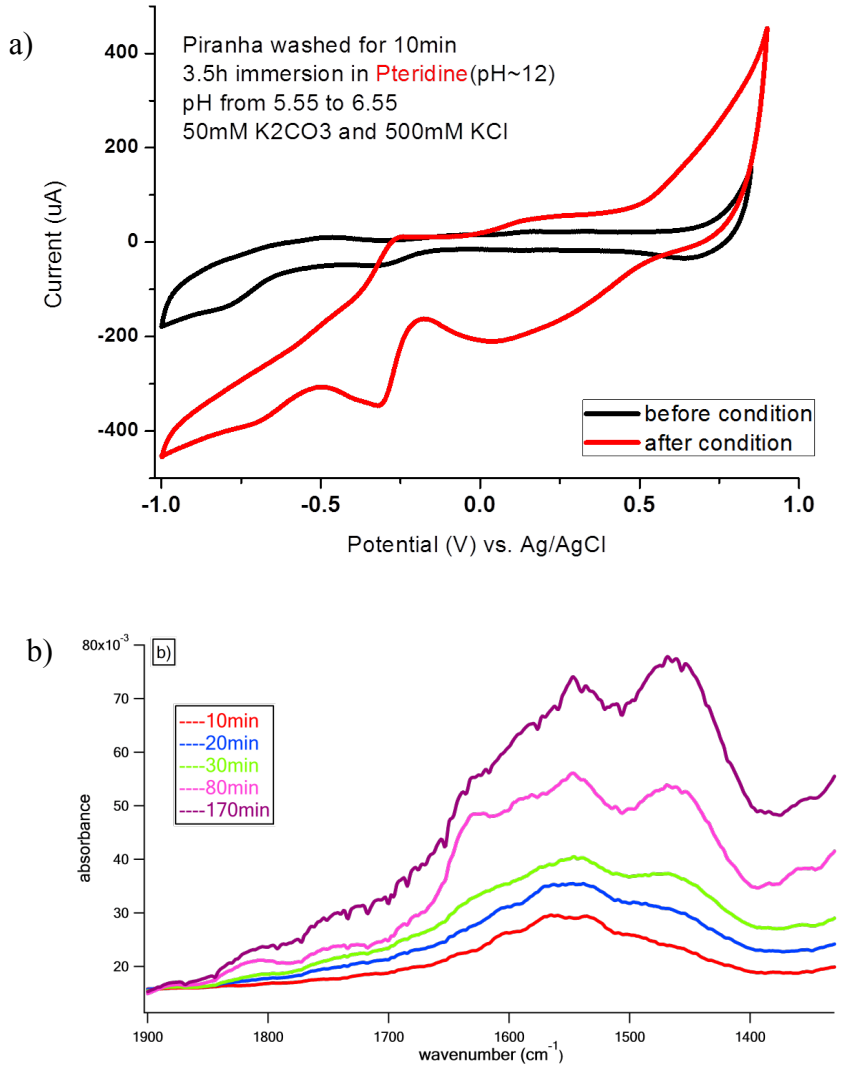

Figure 2.6. a) Cyclic voltammograms of PTE-Au film before and after conditioning; b) FTIRs of PTE-Au film at different time during conditioning (50 mM carbonate solution in D_2O)

Figure 2.7 below shows the gas chromatogram of products after 15 min conditioning and 60 min conditioning of PTE-attached gold electrode in 100 mM carbonate solution at pH 5. After 15 min reaction, the products are closer to $2e^-$ reduced product formic acid

and $4e^-$ reduced product formaldehyde. However, after 60 min reaction, the products are closer to formaldehyde and methanol. Thus, it proves that PTE is indeed a catalyst which can drive the full $6e^-$ reduction from carbonate to methanol. More work needs to be done to test the catalytic efficiency.

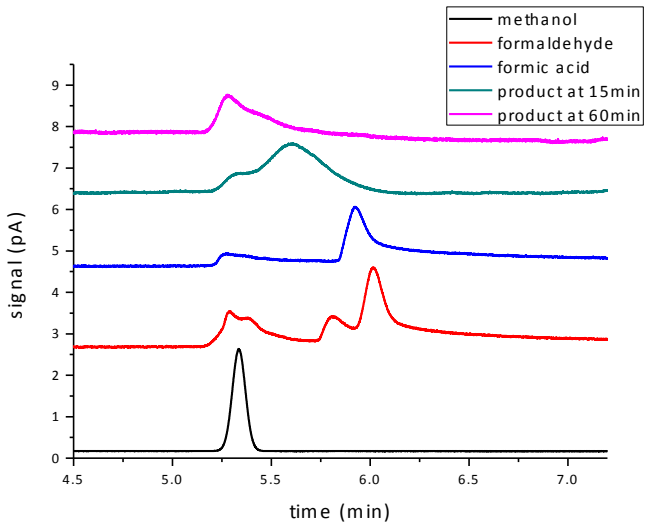

Figure 2.7. GC of methanol, formaldehyde, formic acid, and products after 15 min-conditioning and 60 min-conditioning of PTE-attached Au in 100 mM carbonate solution under pH 5

2.4. Conclusion

We tested the redox chemistry of the three pyridine and its derivatives in bulk solution and studied the redox reactions of mercaptopteridine and it also shows a catalytic CO_2 reduction behavior. Some preliminary investigation (FTIR, GC) of electrocatalyst

attached gold films showed evidence of the formation of formate (formic acid), formaldehyde and methanol.

References

1. (a) Hansen, J.; Sato, M.; Ruedy, R.; Nazarenko, L.; Lacis, A.; Schmidt, G. A.; Russell, G.; Aleinov, I.; Bauer, M.; Bauer, S.; Bell, N.; Cairns, B.; Canuto, V.; Chandler, M.; Cheng, Y.; Del Genio, A.; Faluvegi, G.; Fleming, E.; Friend, A.; Hall, T.; Jackman, C.; Kelley, M.; Kiang, N.; Koch, D.; Lean, J.; Lerner, J.; Lo, K.; Menon, S.; Miller, R.; Minnis, P.; Novakov, T.; Oinas, V.; Perlwitz, J.; Perlwitz, J.; Rind, D.; Romanou, A.; Shindell, D.; Stone, P.; Sun, S.; Tausnev, N.; Thresher, D.; Wielicki, B.; Wong, T.; Yao, M.; Zhang, S., Efficacy of climate forcings. *J Geophys Res-Atmos* **2005,** *110* (D18); (b) Hansen, J.; Sato, M.; Russell, G.; Kharecha, P., Climate sensitivity, sea level and atmospheric carbon dioxide. *Philos T R Soc A* **2013,** *371* (2001).

2. Cole, E. B.; Lakkaraju, P. S.; Rampulla, D. M.; Morris, A. J.; Abelev, E.; Bocarsly, A. B., Using a One-Electron Shuttle for the Multielectron Reduction of CO_2 to Methanol: Kinetic, Mechanistic, and Structural Insights. *J Am Chem Soc* **2010,** *132* (33), 11539-11551.

3. (a) Maden, B. E. H., Tetrahydrofolate and tetrahydromethanopterin compared: functionally distinct carriers in C-1 metabolism. *Biochem J* **2000,** *350*, 609-629; (b)

Xiang, D. M.; Magana, D.; Dyer, R. B., CO_2 Reduction Catalyzed by Mercaptopteridine on Glassy Carbon. *J Am Chem Soc* **2014,** *136* (40), 14007-14010.

4. (a) Boisselier, E.; Astruc, D., Gold nanoparticles in nanomedicine: preparations, imaging, diagnostics, therapies and toxicity. *Chemical Society reviews* **2009,** *38* (6), 1759-1782; (b) Love, J. C.; Estroff, L. A.; Kriebel, J. K.; Nuzzo, R. G.; Whitesides, G. M., Self-Assembled Monolayers of Thiolates on Metals as a Form of Nanotechnology. *Chem Rev* **2005,** *105* (4), 1103-1170.

5. (a) Ferretti, S.; Paynter, S.; Russell, D. A.; Sapsford, K. E.; Richardson, D. J., Self-assembled monolayers: a versatile tool for the formulation of bio-surfaces. *TrAC Trends in Analytical Chemistry* **2000,** *19* (9), 530-540; (b) Motesharei, K.; Myles, D. C., Molecular Recognition on Functionalized Self-Assembled Monolayers of Alkanethiols on Gold. *J Am Chem Soc* **1998,** *120* (29), 7328-7336; (c) Kumar, A.; Biebuyck, H. A.; Whitesides, G. M., Patterning Self-Assembled Monolayers: Applications in Materials Science. *Langmuir* **1994,** *10* (5), 1498-1511.

Chapter 3. CO_2 Reduction Catalyzed by Mercaptopteridine on Glassy Carbon

http://pubs.acs.org/doi/abs/10.1021/ja5081103

3.1. Introduction

The increased carbon emission due to human activity has called attention to the need for a carbon neutral energy cycle. At the same time, the majority of energy consumed by human society is from fossil fuels, which are a limited resource. If we can covert the huge feedstock of carbon dioxide to useful fuels, we can alleviate both the climate change and energy sustainability issues.

However, CO_2 is an extremely stable linear molecule and requires large reorganization energy to bend it, with a change of hybridization from sp^2 to sp^3. The electrochemical reduction of CO_2 usually requires large overpotential. Lots of research has been done focusing on the electrochemical and photochemical catalysts of CO_2 reduction, and the majority of the catalysts are metal-based, as discussed in Chapter 1.

The Bocarsly group reported pyridinium as a one-electron shutter which conducted 6-electron reduction of CO_2 to methanol on platinum electrode with low overpotential.[1] His work has spurred many theoretical and experiment studies on relative systems.

In addition, pterins, as natural cofactors in a wide range of enzymes, function as the redox mediators and C1 carriers. Methanogenesis in archaeal anaerobes depends on pterin cofactors such as methanopterin (MPT).[2] In the process of converting CO_2 to methane, CO_2 is loaded at N5 of the reduced MPT, which can act as the only cofactor involved in the critical steps.[3] Moreover, the active form of pterin can be produced electrochemically.[4]

Therefore, we investigated the potential for 6,7-dimethyl-4-hydroxy-2-mercaptopteridine to act as an electrocatalyst for CO_2 reduction.

3.2. Experiment section

3.2.1. Chemical and material

5 mM 6,7-dimethyl-4-hydroxy-2-mercaptopteridine (PTE) (Sigma Aldrich), in addition to 100 mM potassium chloride (KCl, EMD) works as supporting electrolyte. The solution was degassed by Argon for 30 min and maintained at pH observed under Ar or CO_2.

Other chemicals used are 2,4-Diamino-6-(hydroxymethyl)pteridine (Pte(II)) (Sigma Aldrich) and folic acid (Sigma Aldrich).

3.2.2. Electrochemistry set-up

Cyclic voltammetry and bulk electrolysis measurements were performed on a Reference 3000 Potentiostat/ Galvanostat/ZRA (Gamry Instruments).

For the cyclic voltammetry experiment, a three-neck flask was used as electrochemical cell and a platinum wire (MW-4130, BASi) and Ag/AgCl (3 M NaCl) electrode (MF-2052, BASi) were counter electrode and reference electrode, respectively. Glassy carbon (MF-2012, BASi), gold (MF-2014, BASi) and platinum (MF-2013, BASi) were all used as working electrode. Every electrode was polished with 1μm alumina before use. The efficient surface area of gold electrode (0.1035 cm^2) and platinum electrode (0.1035 cm^2) were obtained from the oxygen desorption and hydrogen desorption peak, respectively, in 0.5 M H_2SO_4 solution. The geometric surface area (0.07069 cm^2) was used as the real surface area for glassy carbon electrode. The scan rate is 100 mV/s if not specified.

Bulk electrolysis was conducted in the BASi bulk electrolysis cell, using the reticulated vitreous carbon electrode (RVC, MF-2077, BASi) as working electrode, Coiled Platinum (MW-1033) as Auxiliary Electrode, and Ag/AgCl (3 M NaCl) electrode (MF-2052, BASi) as reference electrode.

The rotating disk electrode (RDE) experiment was conducted on Pine AFMSRCE rotator. The working electrode was glassy carbon HotSpot RDE tip (5 mm disk OD) (AFE3T050GCPK).

3.2.3. FTIR set-up

Labview was used to synchronize the FTIR to the potentiostat providing the ability to change the potential and collecting the 128 scans at 2 cm^{-1} resolution. The FTIR spectra

are collected using Varian 3100 FTIR spectrometer equipped with liquid nitrogen cooled mercury cadmium telluride (MCT) detector. The sample solution in the electrochemical cell was flowed to the transmission cell by using Rabbit-HP solvent delivery system (Rainin Instrument Co. Inc.). The path length is 50 μm. The scheme of this set-up is shown in Figure 3.1.

3.2.4. NMR

The ^{13}C NMR data were obtained using an Innova 600 MHz instrument with 10 hrs signal averaging with a relaxation time set at 2.5 s at room temperature, with $^{13}CO_2$ as reference. 10% D_2O was used to lock the NMR instrument.

3.2.5. Gas chromatography

The GC data were obtained with an Agilent Model 7890A GC equipped with VICI pulsed discharge detector, an Agilent HP-PLOT/U column, inlet pressure 10 psi, split ratio 100:1, oven temperature 120 °C and manual injection of 0.2 μL of reaction solution. The solution was initially passed through a preequilibrated Amberlite IRN-150 ion exchange column to remove ionic species (electrolyte, formate) before injection onto the GC column to protect the column from damage.

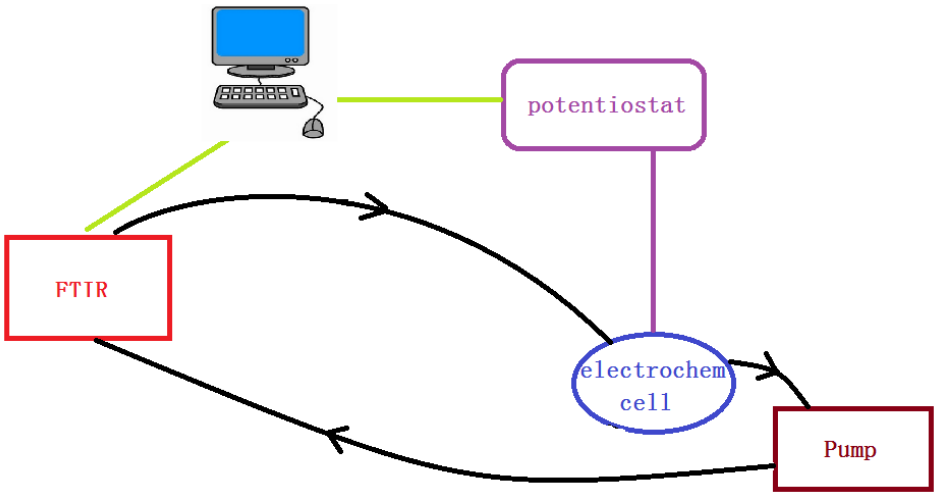

Figure 3.1. Scheme of the electrochemistry-FTIR set-up

3.3. Results and discussion

3.3.1. Cyclic Voltammetry of PTE

3.3.1.1. Redox of PTE

The resonance structure of PTE is shown in Figure 3.2a, displaying an equilibrium between the hydroxyl form and a ketone form. Another possible tautomer is the thiouracil form according to personal discussion with Charles B. Musgrave (University of Colorado Boulder). PTE shows two electron redox chemistry on all of Au, Pt and glassy carbon electrodes, as shown in Figure 3.2, in agreement with previous work.[4] It also makes sense chemically because the 1 e^- reduced species (radical) will be unstable and highly reactive, leading to disproportionation and other possible pathways. The overpotential decreases from Pt to glassy carbon to Au electrode, as well as the reversibility of the redox pair. However, it shows largest current density on glassy carbon electrode.

3.3.1.2. PTE electrocatalysis

CO_2 reduction catalyzed by PTE is observed at a low overpotential on glassy carbon electrode, without the involvement of any metals. The electrochemistry of PTE on glassy carbon under Ar atmosphere (also pre-saturated with Ar gas) is quasi-reversible with a two-electron redox couple centered at −0.68 V vs Ag/AgCl (3M), as shown in Figure 3.3a (blue curve). In contrast, when the solution is saturated with CO_2, a catalytic wave is observed (red curve), characterized by significantly greater current flow and irreversible reduction (Figure 3.3a), which indicates the reduction of CO_2. In addition, CO_2 reduction does not occur in the absence of PTE (black curve). A catalytic reduction wave is also observed starting with formic acid in the presence of PTE, as shown in Figure 3.3b, while no reduction of formic acid is observed without the PTE catalyst (Figure 3.3b, black curve). These results suggest that PTE has the potential to act as a single, multifunctional catalyst for successive two-electron reduction steps of CO_2, i.e., from CO_2 to formic acid and then to formaldehyde or further reduced products.

a)

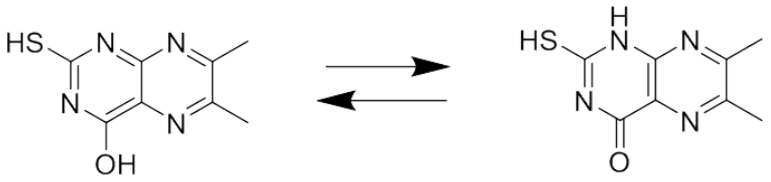

6,7-dimethyl-4-hydroxy-2-mercaptopter 6,7-dimethyl-4-hydroxy-2-mercaptopteridine **(PTE)**

b)

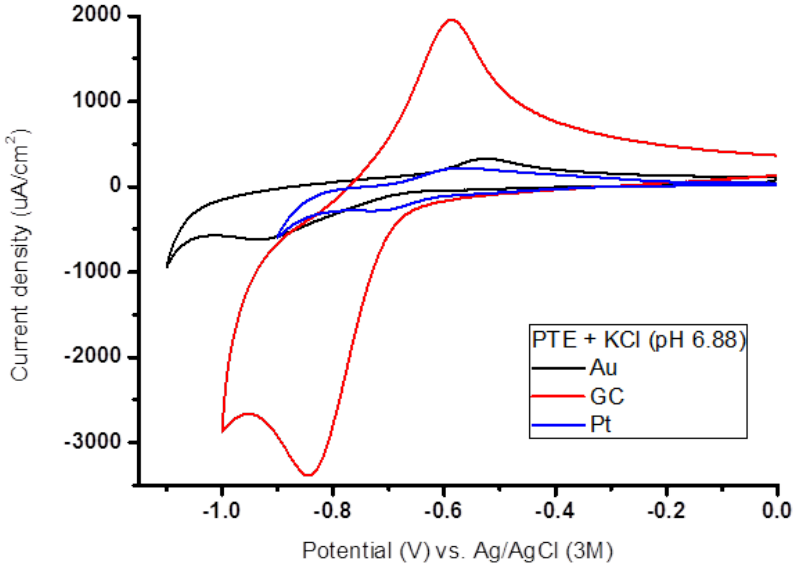

Figure 3.2. (a) Equilibrium structures of PTE; (b) Cyclic voltammetry of 20 mM PTE on different electrodes: Au, Pt and glassy carbon (GC) electrode (0.1M KCl as supporting electrolyte, scan rate 100 mV/s, pH 6.88)

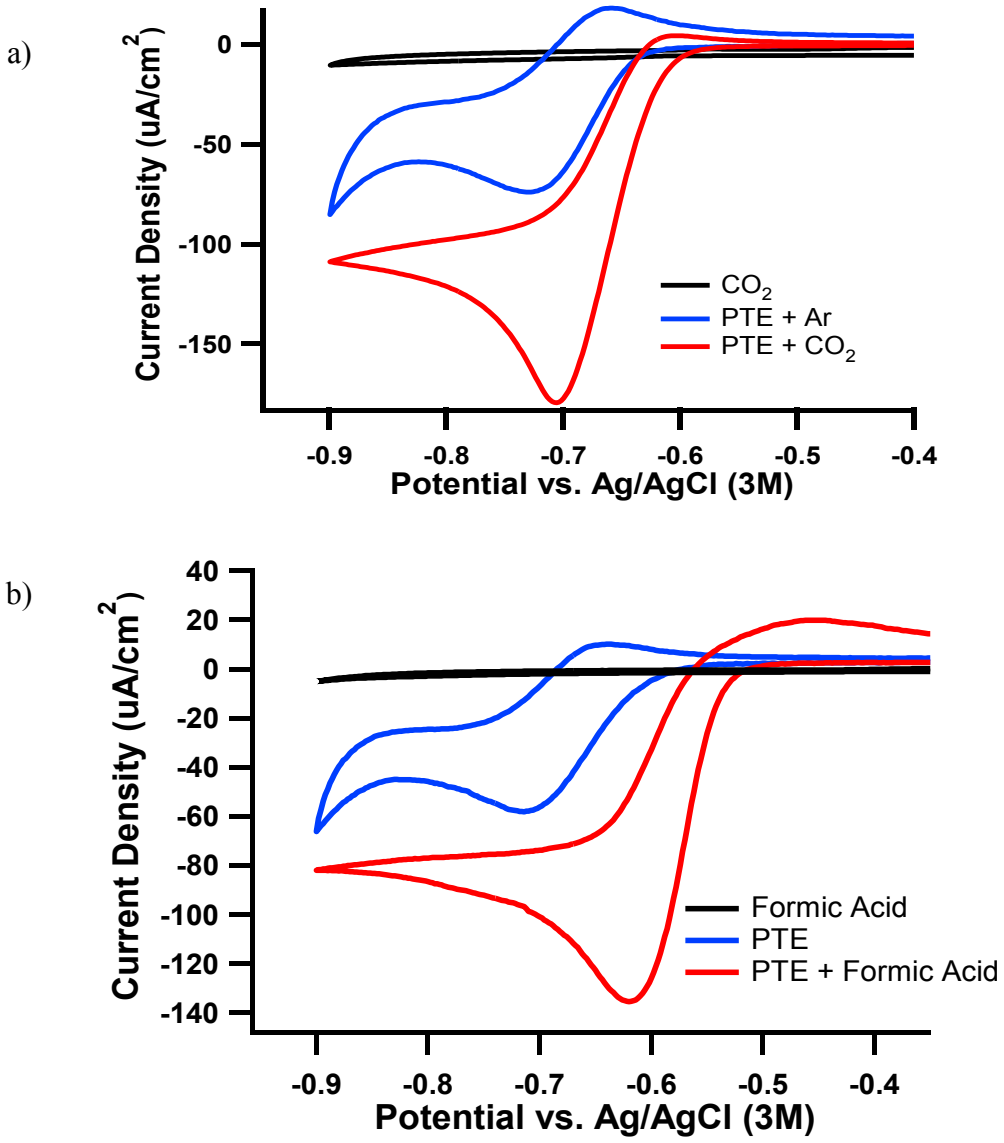

Figure 3.3. PTE electrocatalysis. (a) Cyclic voltammograms of saturated CO_2 solutions with (red) and without (black) PTE catalyst on a glassy carbon electrode. PTE alone under Ar is shown for comparison (blue). Conditions: 10 mM PTE, 100 mM KCl (pH 6.3), scan rate of 1 mV/s. (b) Cyclic voltammograms of 33 mM formic acid with (red) and without (black) PTE on a glassy carbon electrode in 100 mM KCl solution at pH 4.6 and 4.2, respectively.[5]

The scan rate of Figure 3.3 is 1 mV/s and other conditions are the same, and the only difference is the pre-saturated gas atmosphere, either Ar or CO_2. Direct comparison under the same conditions controls for the possibility of convection because it should be the same in both cases (convection of dissolved CO_2 related species will not make such a big change in current density). To further prove this, we conducted cyclic voltammetry at faster scan rates, as shown in Figure 3.4. At scan rates of 5 mV/s and 50 mV/s, the catalytic CO_2 reduction curve (red traces) are still observed, which show significant

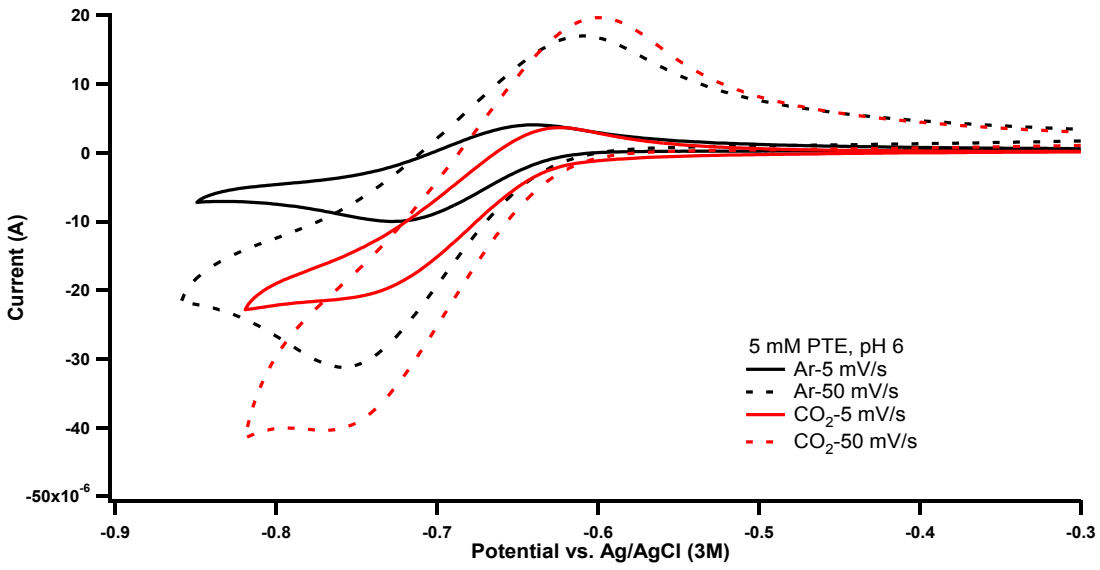

Figure 3.4. Cyclic voltammograms of saturated CO_2 solutions (red) or under Ar (black) of 5 mM PTE, pH 6.0, 0.1 M KCl, at the indicated scan rates.

enhancement compared with the PTE redox chemistry under Ar atmosphere (black traces). Furthermore, unlike the case of experiments on a Pt electrode, this enhanced current is not due to proton reduction since this process has a high overpotential on glassy carbon. There are no bubbles (H_2) forming on the electrode surface during this process, which means the proton reduction is not contributing to the observed excess current flow.

3.3.1.3. pH dependence

All of the pH dependence experiments of PTE redox were conducted under Ar atmosphere. When pH decreases from 8.66 to 1.99, the two- electron redox peaks (Pc1) of PTE centered between -0.7 V and -0.8 V decreases as well and another peak (Pc2) centered between -0.4 V and -0.5 V appears gradually (Figure 3.5a). The Bocarsly group observed a similar pattern for pyridine species on platinum electrode, and he assigned the reduction peak at lower pH to H_3O^+ reduction.[6] However, hydrogen evolution has a high overpotential on glassy carbon electrode. Figure 3.5b shows the comparison of the cyclic voltammetry of KCl electrolyte solution with and without PTE on glassy carbon electrode under acidic pH. In the absence of PTE, there are no redox peaks at all, indicating Pc2 must relate with PTE as well. In addition, no H_2 was detected in the product characterization of bulk electrolysis conducted at this pH. Therefore, Pc2 should not be H_3O^+ reduction in this case. According to Dryhurst, this new peak can be assigned to the 2 H^+-2 e^- reduction from the quinonoid form to tetrahydropteridine as shown in Fig. 1.7.[4]

a)

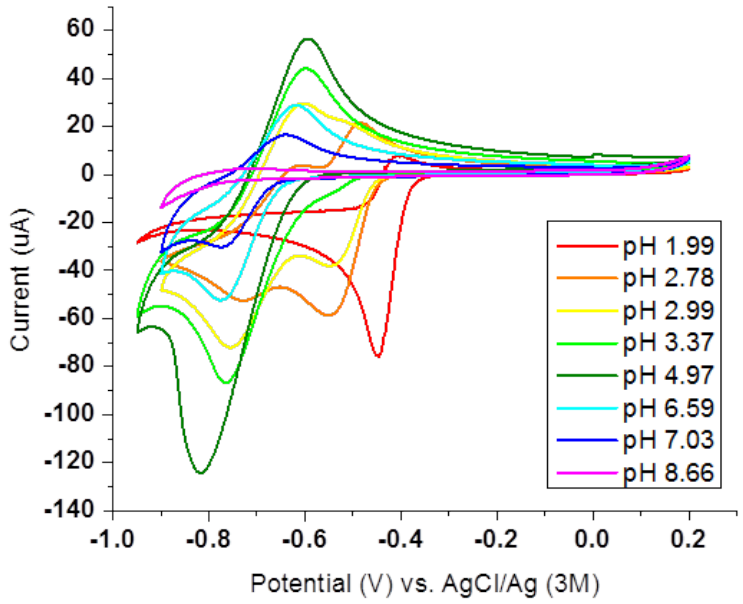

b)

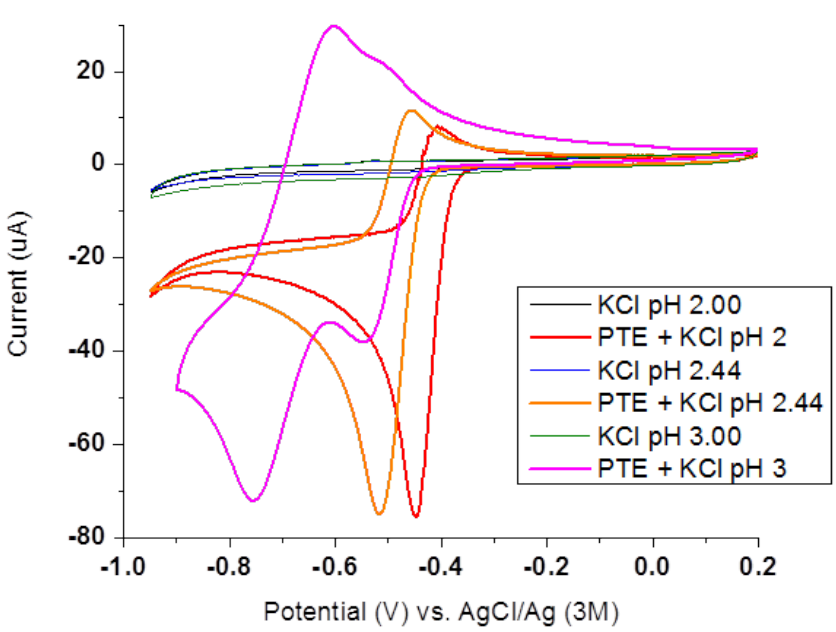

Figure 3.5. Cyclic voltammetry of (a) PTE at different pH. (b) PTE/KCl vs. KCl at different pH. (10 mM PTE, 0.1 M KCl)

3.3.1.4. Salt concentration dependence

At pH 7, the redox pair of PTE shows larger current in 100 mM KCl solution compared with 200 mM KCl, which can be explained by the influence of local pH at the electrode surface. When at high supporting electrolyte concentration, there are more K^+ ions competing with H^+ near the electrode surface, resulting in less H^+ availability, thus the reduction current of the $2H^+$-$2e^-$ process is decreased. This is quite important because protons are needed to both reduce the catalyst and CO_2. In the limit where electron

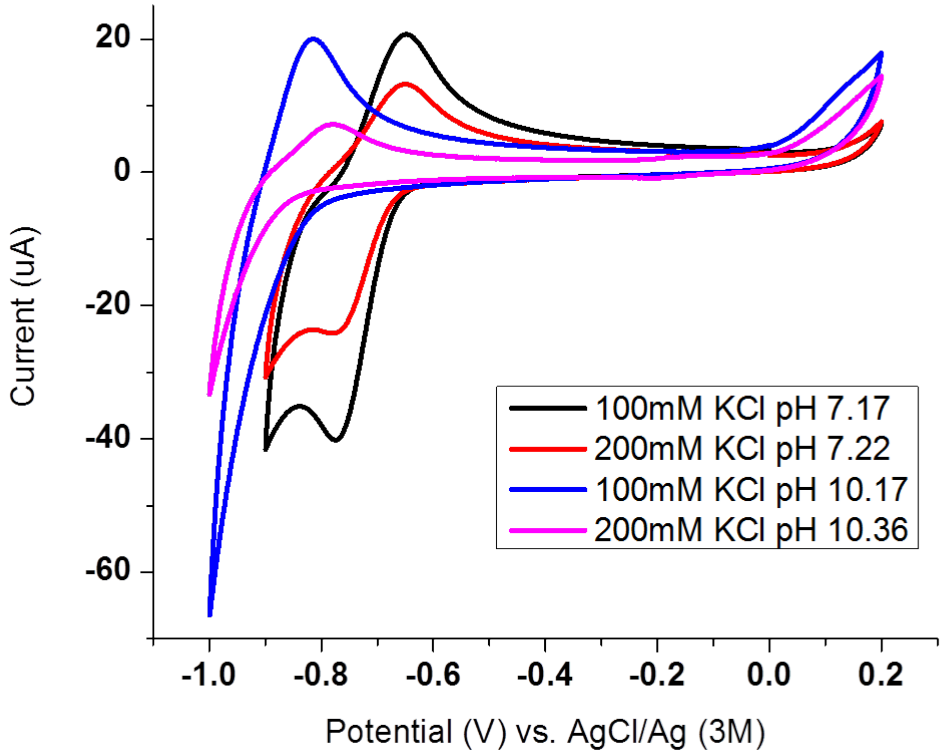

Figure 3.6. Cyclic voltammetry of PTE on glassy carbon electrode in solution with different KCl concentration

transfer from the electrode is rapid, the proton transfer step might become the rate limiting step, especially as protons near the interface become depleted.

3.3.2. FTIR spectroelectrochemistry

Bulk electrolysis was conducted using a reticulated vitreous carbon (RVC) electrode as the working electrode. The sample solution from the electrochemical cell is flowed into an infrared transmission cell during bulk electrolysis to follow the progress of the electrocatalytic reaction, in order to identify products formed in the electrochemical reaction and if possible, to identify any intermediate species. Figure 3.7 shows the FTIR difference spectra (spectra at indicated potentials minus the spectrum at no applied potential) of PTE under (a) Ar or (b) CO_2 atmosphere and (c) the simulated spectrum using reference spectra of the products. The spectrum of unreduced PTE is also shown in Figure 3.7(a) for comparison. Under Ar atmosphere, the reduction of PTE leads to a progressive bleach of the ground-state bands as the potential is scanned more negative, as well as a concomitant buildup of positive features. As characteristic of pterin reduction, all absorbance are shifted to lower frequency. [7] The ketone absorbance at 1690 cm^{-1} is only slightly shifted to 1679 cm^{-1} upon reduction. However, the pyrazine C=N mode, which is at 1512 cm^{-1}, disappears, which indicates the reduction of the pyrazine ring, consistent with two-electron electrochemical reduction.[4] The same experiment is repeated with solution which is pre-saturated with CO_2. When the potential scans toward more negative, similar bleach features due to reduction of PTE are present. Meanwhile, a progression of new peaks is observed, resulting from the reduction of CO_2. At the

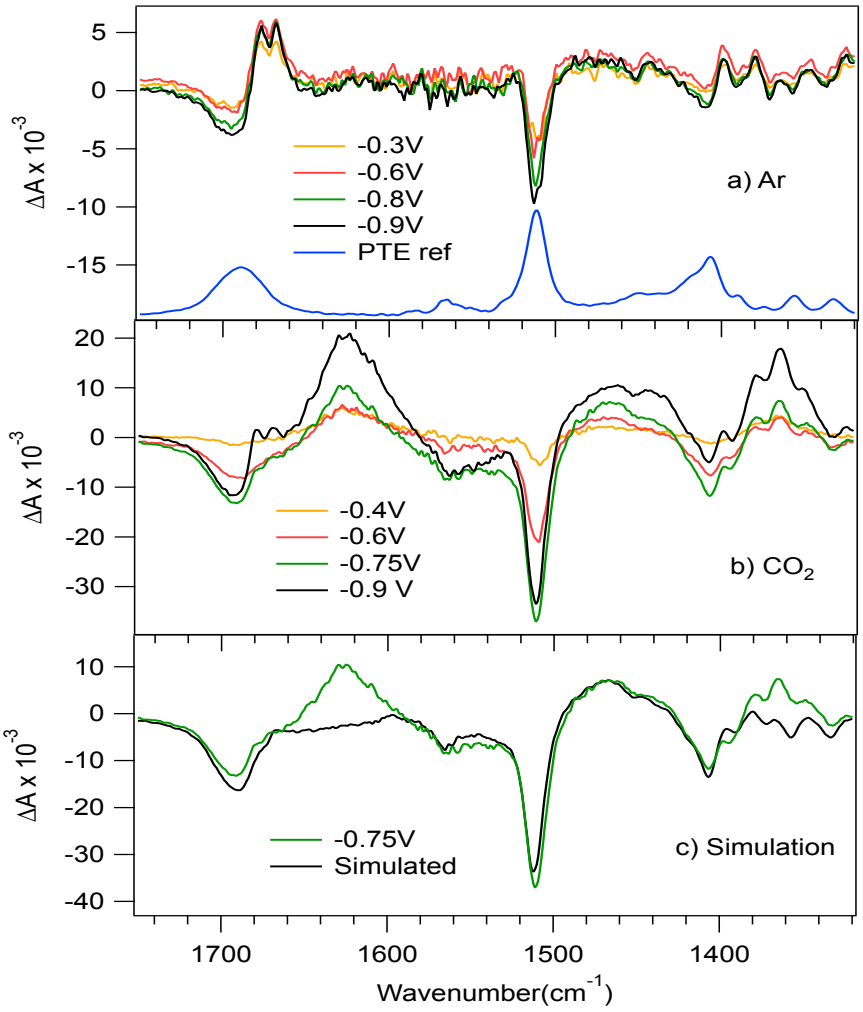

Figure 3.7. FTIR analysis of bulk electrolysis reactions (scan rate of 1 mV/s, RVC working electrode). (a, b) Difference FTIR spectra (spectra at indicated potentials minus the spectrum at no applied potential) of PTE under (a) Ar and (b) saturated CO_2 solutions scanned at 1 mV/s. (c) Simulated spectrum from reference spectra in D_2O[5]

potential of -0.4 V, the bleach of ketone appears, while the corresponding positive feature is missing, which suggests the fast reaction of reduced PTE with CO_2 that is not detected

on the 1-2 min time scale of the FTIR experiment. The simulation of IR difference spectra (Figure 3.7c) is obtained using a linear combination of the reference spectra of potential products in D_2O, and subtracting the ground state PTE spectrum (appendix 1, figure A3.1). The FTIR spectrum at -0.75 V in CO_2 pre-saturated solution (green trace in figure 3.7b) fits the simulation best with a combination of formate:formaldehyde:methanol product at a ratio of 2:1.5:1. The major absorbances of methanol (1466 cm^{-1}), formaldehyde (1442 cm^{-1}) and formate (1350 and 1370 cm^{-1}) are all well-fit in this simulation. However, the most prominent discrepancy between the simulation and real spectrum is that the broad peak of 1625 cm^{-1} which is present in the experimental spectrum. As a hypothesis, we assign this peak to a Pteridine-CO_2 carbamate intermediate formed by the addition of CO_2 to one of the nitrogens on the reduced pyrazine ring, by analogy to the IR spectra of known carbamates. [8] In figure 3.7b, buildup of the reduced PTE is also observed at the lowest potential (−0.9 V) in CO_2 pre-saturated solution experiment, as evidenced by the appearance of the positive peak at 1679 cm^{-1} (the ketone absorbance of two-electron-reduced PTE), which may be related to the accumulation of the reduced PTE at this potential, resulting from faster catalysis and depletion of CO_2 in the solution.

3.3.3. Product analysis: GC and NMR

Bulk electrolysis of a saturated CO_2 solution containing the PTE catalyst in 100 mM KCl at pH 6.3 (100 mM phosphate buffer) was conducted for ~2 h at −0.65 V (vs Ag/AgCl (3M)), the products were detected by gas chromatography and ^{13}C NMR spectroscopy, both of which proved the formation of methanol, as shown in figure 3.8[5]. In contrast, no methanol was detected when the solution was under Ar atmosphere or

without the presence of PTE. Figure 3.8c is the ^{13}C NMR spectrum for the bulk electrolysis of a $^{13}CO_2$ saturated solution, which was conducted under a slight positive pressure of $^{13}CO_2$ and the solution was re-circulated using a peristaltic pump to maintain gas saturation. ^{13}C NMR shows peaks at 48 and 171 ppm due to ^{13}C-enriched methanol and formate, respectively, demonstrating that the origin of these products is from CO_2 reduction. The most intense peaks are due to unreacted ^{13}C labeled CO_2 and bicarbonate.

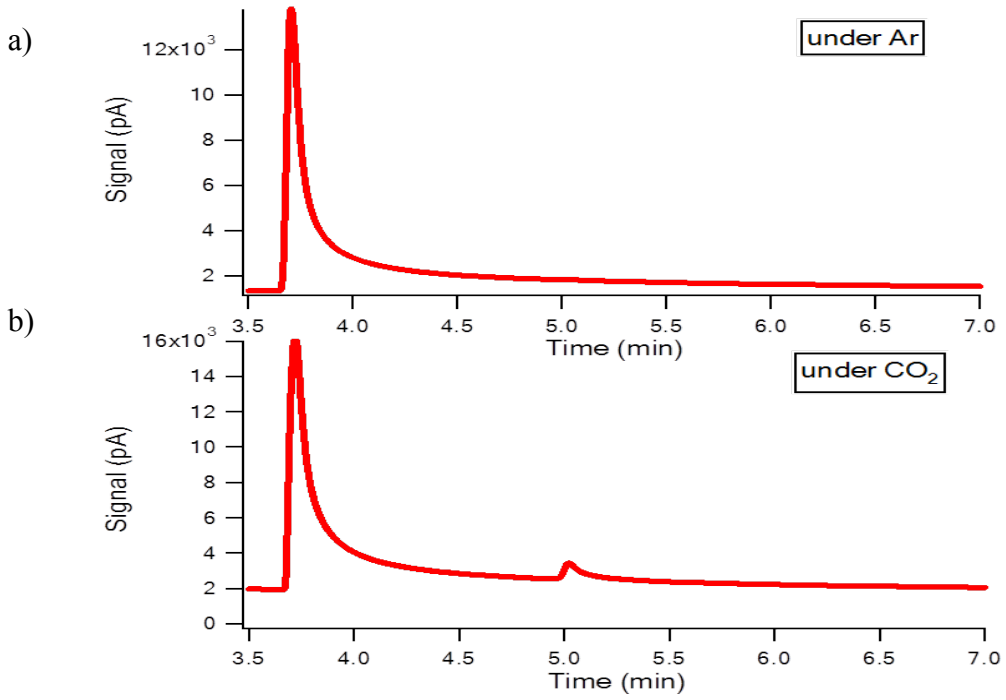

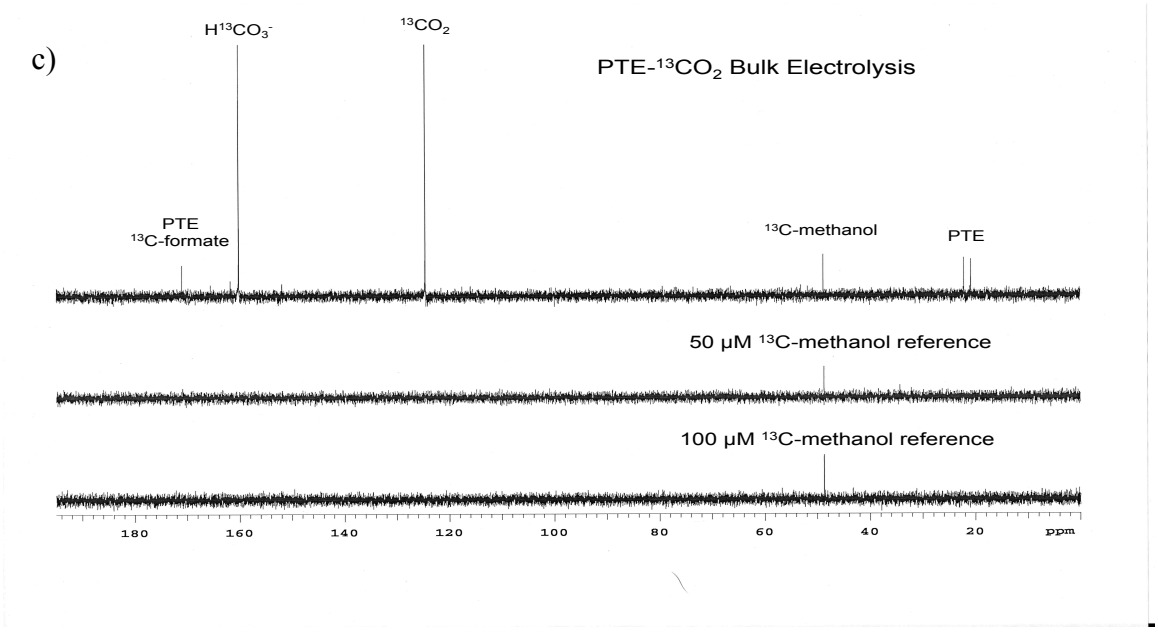

Figure 3.8. Bulk electrolysis product analysis**.** Gas chromotography under (a) Ar (b) CO_2 atmosphere. (c) C^{13} NMR (Top) of product solution of $^{13}CO_2$ saturated solution containing the PTE catalyst (5 mM).

PTE peaks are also observed even though the catalyst is not ^{13}C labeled, because it is present at 5 mM and therefore gives significant intensity compared to the ~100 μM ^{13}C labeled methanol produced in the electrocatalysis. However, the intensity of the ^{13}C NMR peaks depends on the relaxation times and other parameters and is therefore not simply related to the concentration. Spectra for reference solutions of methanol in D_2O are shown below for comparison.

The concentration of product methanol is obtained via gas chromatography through standard concentration calibration (Appendix 1 figure 3A.2), which indicated that the

Faradaic efficiency of methanol formation is between 10−23%. The Faradaic efficiency is given by: ([MeOH]*6e-)/i•t, where i•t is the integrated bulk electrolysis current.

3.3.4. Proposed mechanism

Based on the discussion above, PTE can act as a single catalyst for multiple electron reduction of CO_2. The FTIR data indicates carbamate as a possible intermediate. Combining the discussion in section 1.3 and 1.4, we postulate the mechanism as below in figure 3.9. PTE first gets reduced to its active form H_2PTE, and then CO_2 loads at N5 position of H_2PTE, forming H_2PTE-CO_2 carbamate as an intermediate, followed by HT-PT process to generate formic acid. It works the same way to produce formaldehyde and methanol. In this proposed mechanism, hydride transfer is the centerpiece, by analogy to the mechanism of pterin cofactors functioning in biological systems. Here, the hydride transfer is probably intramolecular transfer from C4 to the carbamate.

3.3.5. Kinetic isotope effect (KIE)

One way to verify the hydride transfer mechanism is to measure the kinetic isotope effect, i.e., the H/D KIE on the hydride transfer step. However, to measure this directly we would have to follow the hydride transfer itself, which will be difficult. But if hydride transfer is the rate limiting step, the steady state kinetics should show a substantial H/D KIE. In addition, if there are PCET reactions at any step (and there almost certainly are), the reactions should show a KIE. Therefore, it is quite challenging to sort out whether the

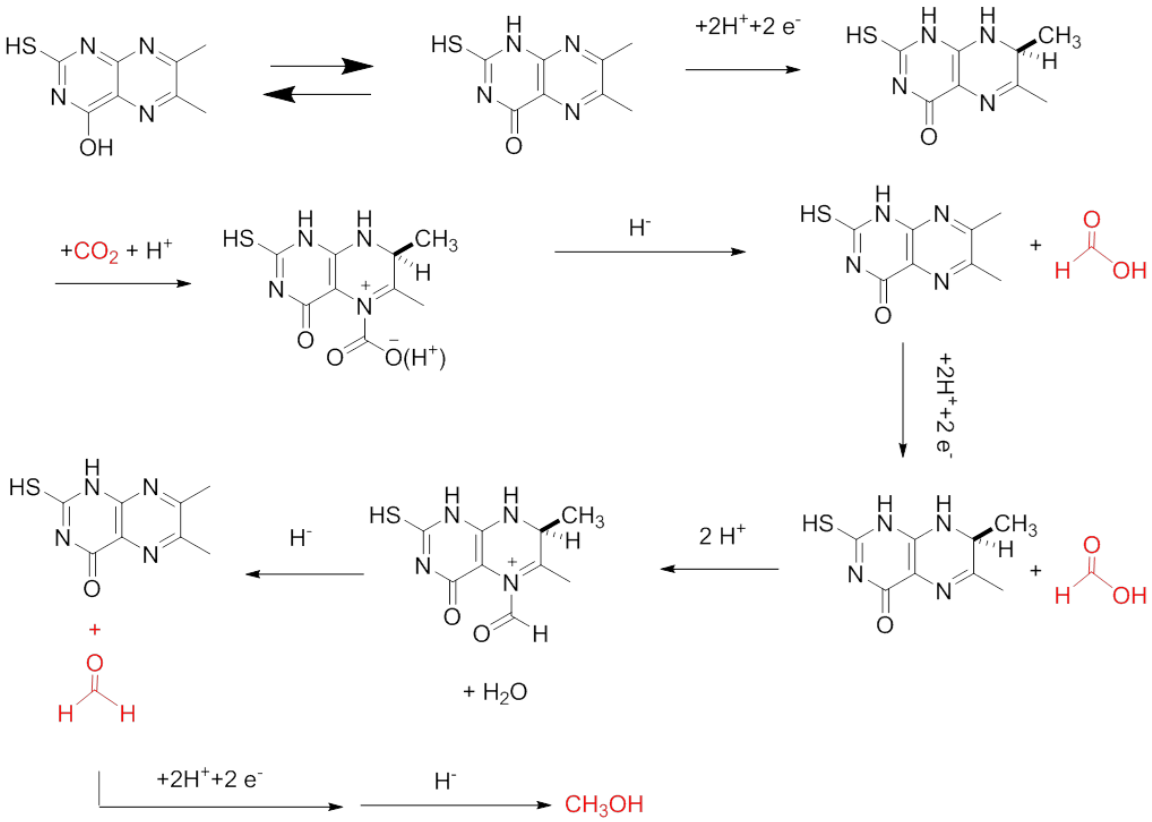

Figure 3.9. Proposed mechanism of CO_2 reduction catalyzed by PTE

observed KIE is due to hydride transfer or PCET. Figure 3.10 shows the cyclic voltammetry of PTE in H_2O sand D_2O solution, pre-saturated with Ar and CO_2. In H_2O solution (red traces), as aforementioned, it shows enhanced catalytic current under CO_2. Because of the faster scan of 100 mV/s, the enhancement is not as big as data shown in section 3.2.1.2 and 3.2.1.3. Similar enhancement pattern also is observed in D_2O solution. The comparison of the cyclic voltammetry under Ar in H_2O and D_2O solution (solid lines) shows the latter one has 50 mV more overpotential. When under CO_2 (dashed lines) the overpotential difference is as large as 180 mV. Cyclic voltammetry is a transient technique and is sensitive to the kinetics. So the difference in observed midpoint

potentials may be due to the kinetics (although the thermodynamics might also contribute, since the solvent is involved in both the ET and PT reactions). A key observation is that the apparent reduction potential of PTE under Ar shifts more negative in D_2O. This probably means the reduction involves PCET, such that the ET and PT are coupled. The apparent overpotential in D_2O suggests the reduction slows down in D_2O because PT has a lower barrier than DT (the proton has a higher zero point energy than the deuteron, so it has a lower barrier).

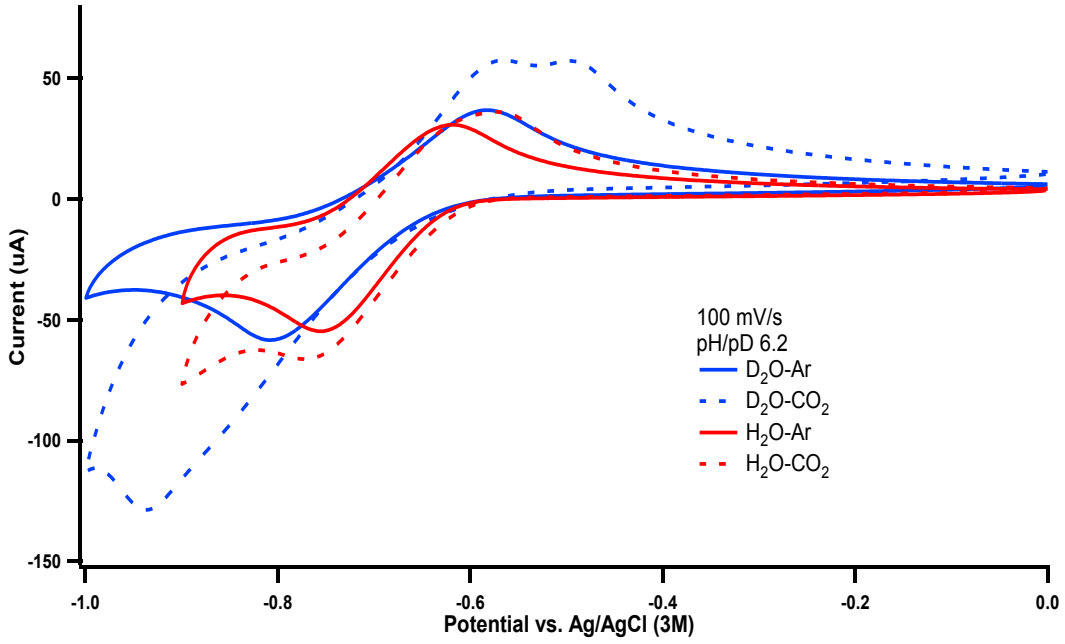

Figure 3.10. Cyclic voltammetry of PTE in H_2O and D_2O solution, pre-saturated with Ar and CO_2 (0.1 M KCl, scan rate 100 mV/s)

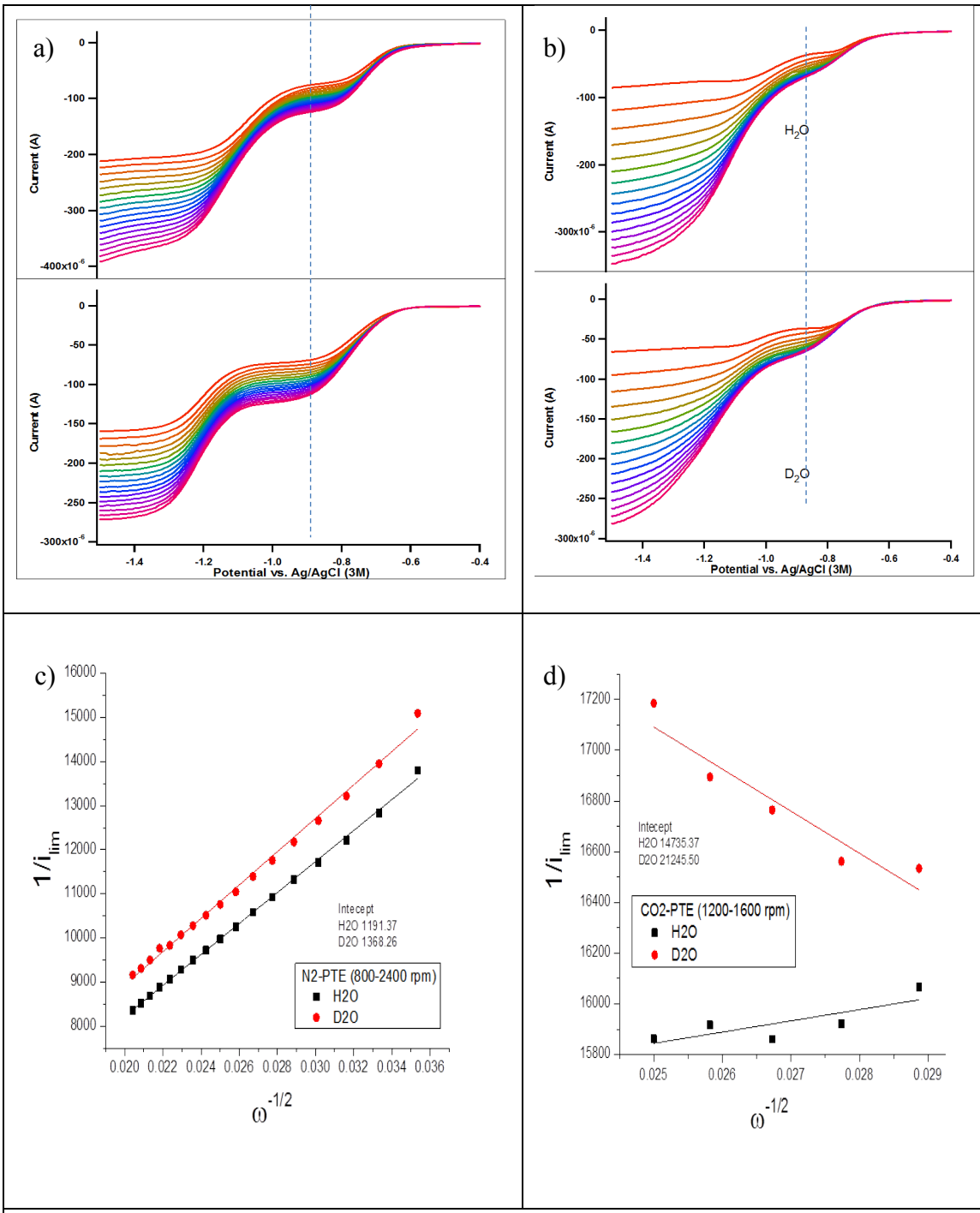

Figure 3.11. Koutecky-Levich rotating disk electrochemistry (RDE). Voltammogram of 4 mM PTE presaturated and under the atmosphere of (a) N_2 and (b) CO_2. Koutecky-Levich plot under (c) N_2 and (d) CO_2. (0.1 M KCl, glassy carbon electrode, scan rate of 50 mV/s)

To quantify the KIE, initial Koutecky-Levich rotating disk electrochemistry (RDE) was conducted in order to get the heterogeneous rate constant of the electrochemical reaction. Figure 3.11a and 3.11b show the voltammograms of PTE in both H_2O and D_2O under Ar and CO_2 respectively. The two reduction processes were observed, which is consistent with the electrochemistry study of pterin.[4] The reduction wave centered around -0.8 V is the one with interest. Koutecky-Levich plots of this reduction wave are shown in Figure 3.11c and 3.11d.

According to the Koutecky-Levich equation below, the rate constant k^0 can be calculated under each condition.

$$1/i_{lim} = 1/i_k + 1/(0.2\ n\ F\ A\ D^{2/3}\ \omega^{1/2}\ \upsilon^{-1/6}\ C)$$

$$i_k = n\ F\ A\ k^o\ C$$

Under N_2, k_H/k_D=1.15, while under CO_2, k_H/k_D=1.44. KIE of the CO_2 system is larger than that of the N_2 system, which indicates a possible hydride transfer in the CO_2 system. However, this is just preliminary results which still have some issues to address. First, the electrochemical cell is open to air, and when the working electrode rotates vigorously, there is a high possibility to lose some dissolved CO_2 in the solution. If a CO_2 atmosphere is placed above the electrochemical cell, another issue arises, which is how to maintain the pH. Second, the scan rate of this data is 50 mV/s. As discussed earlier, the enhancement of reduction current at this relatively fast scan rate is not as obvious as the slower scans. The data above are consistent with the reduction of PTE; however, to be able to resolve the subsequent chemistry (very slow), slower scan rates should be applied. It should be noted still that hydride transfer is just one possibility. As aforementioned,

any PCET process should also show an H/D KIE. However, the most likely origin of the H/D KIE is hydride transfer since in this system there is low possibility of single ET processes, because they would produce high energy radical intermediates.

3.3.6. Pte(II) and folic acid

Besides PTE, we also tested other pterin containing compounds, including 2,4-Diamino-6-(hydroxymethyl)pteridine (Pte(II)) and folic acid. Figure 3.12 shows the electrocatalytic results. They both show similar catalytic curve under CO_2, which indicates the potential of other pterin molecules to work as a CO_2 reduction catalyst. What needs to be noted is that the cyclic voltammogram of folic acid shows two reduction peaks at -0.62 V and -0.78 V. Under CO_2, the catalytic current shows at -0.62 V, indicating this is the reduction potential of the active form of folic acid for CO_2 reduction.

3.4. Conclusion

In summary, PTE acts as a molecular electrocatalyst for CO_2 reduction on a glassy carbon electrode. FTIR, NMR and gas chromatography together prove the formation of methanol as a reduction product. We proposed a mechanism including 1) carbamate as an intermediate; followed by 2) multiple hydride transfer processes. As aforementioned, the

active form of PTE for CO_2 reduction is the 2 e^- reduced species. The proposed mechanism avoids one electron

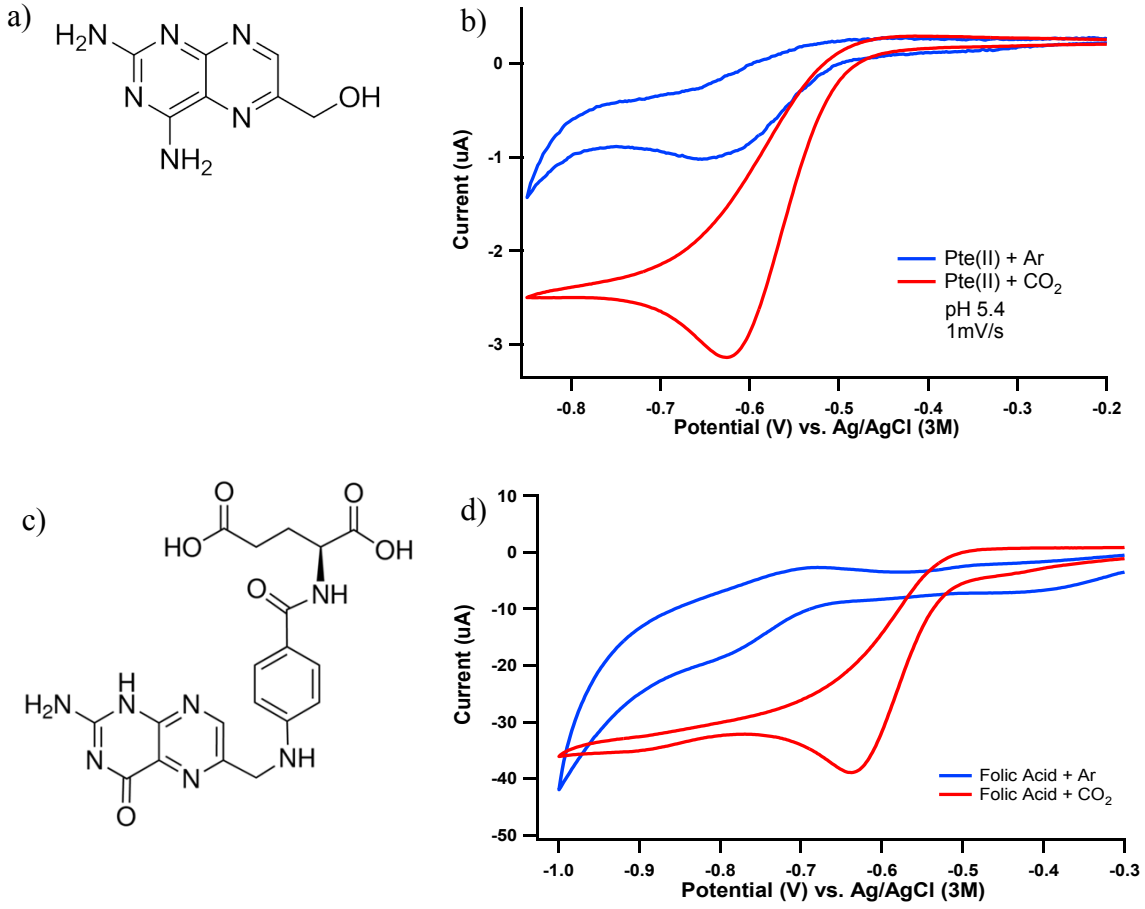

Figure 3.12. Structure (a) and electrocatalysis (b) of Pte(II). Structure (c) and electrocatalysis (d) of folic acid. (0.1 M KCl, scan rate of 1 mV/s, glassy carbon as working electrode)

intermediates, since hydride transfer is effectively a 2 e^- reduction of the C center. Based on a theoretical study, the Musgrave group proposed a concerted $2H^+/2e^-$ transfer to PTE transforms it predominantly into the dihydropteridine tautomer, which reduces CO_2 to CH_3OH via three successive hydride and proton transfers (HTPT). They found that the catalytic ability of dihydropteridine tautomer originates from the de-aromatization of PTE upon its reduction, and the recovery of aromatization as the dihydropteridine tautomer transfers a hydride. Thus, the catalysis is actually driven by a dearomitization-aromatization process. All of the Musgrave's PTE calculation work is obtained via personal communication.

References

1. Cole, E. B.; Lakkaraju, P. S.; Rampulla, D. M.; Morris, A. J.; Abelev, E.; Bocarsly, A. B., Using a One-Electron Shuttle for the Multielectron Reduction of CO2 to Methanol: Kinetic, Mechanistic, and Structural Insights. *J Am Chem Soc* **2010,** *132* (33), 11539-11551.

2. Dimarco, A. A.; Bobik, T. A.; Wolfe, R. S., Unusual Coenzymes of Methanogenesis. *Annu Rev Biochem* **1990,** *59*, 355-394.

3. Maden, B. E. H., Tetrahydrofolate and tetrahydromethanopterin compared: functionally distinct carriers in C-1 metabolism. *Biochem J* **2000,** *350*, 609-629.

4. Dryhurst, G.; Raghavan, R.; Egeserpkenci, D.; Karber, L. G., Electrochemistry of Reduced Pterin Cofactors. *Advances in Chemistry Series* **1982,** (201), 457-487.

5. Xiang, D. M.; Magana, D.; Dyer, R. B., CO_2 Reduction Catalyzed by Mercaptopteridine on Glassy Carbon. *J Am Chem Soc* **2014,** *136* (40), 14007-14010.

6. Yan, Y.; Zeitler, E. L.; Gu, J.; Hu, Y.; Bocarsly, A. B., Electrochemistry of Aqueous Pyridinium: Exploration of a Key Aspect of Electrocatalytic Reduction of CO2 to Methanol. *J Am Chem Soc* **2013,** *135* (38), 14020-14023.

7. Moore, J.; Wood, J. M.; Schallreuter, K. U., Evidence for specific complex formation between alpha-melanocyte stimulating hormone and 6(R)-L-erythro-5,6,7, 8-tetrahydrobiopterin using near infrared Fourier transform Raman spectroscopy. *Biochemistry-Us* **1999,** *38* (46), 15317-15324.

8. Hisatsune, I. C., Low-Temperature Infrared Study of Ammonium Carbamate Formation. *Can J Chem* **1984,** *62* (5), 945-948.

Appendix 1

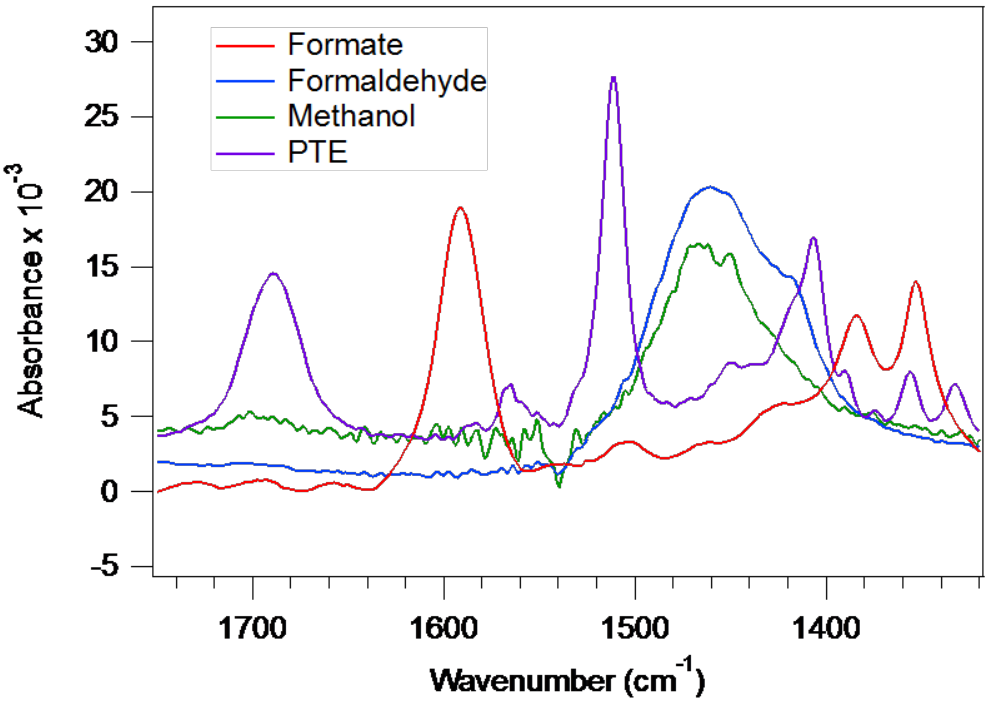

Figure 3A.1. Reference FTIR spectra of formate, formaldehyde, methanol and PTE in D_2O. FTIR spectra were recorded on a Varian 3100 FTIR spectrometer equipped with liquid nitrogen cooled mercury cadmium telluride (MCT) detector, using a transmission IR cell (50 µm pathlength), 2 cm^{-1} spectral resolution and an average of 128 scans. These reference spectra were used to simulate the spectroelectrochemistry difference spectra by fitting to the equation:

$$S = a * fa + b * fl + c * me - d * PTE$$

where *fa, fl, me, PTE* represent the FTIR absorbance spectra of formate, aqueous formaldehyde, methanol and PTE, respectively. The coefficients are adjusted to give the best fit to the FTIR difference spectra.[5]

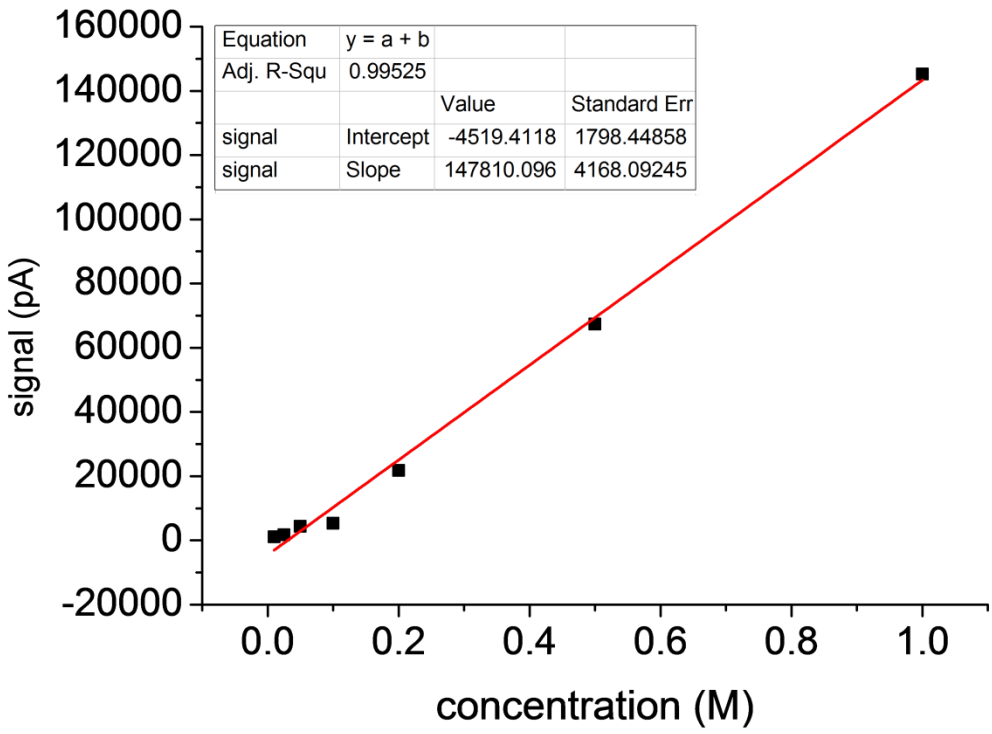

Figure 4. GC calibration of methanol concentration in water, as a plot of the integrated methanol peak at 5 min retention time versus initial methanol concentration. Since the split ratio is 100:1, the detected concentration is 1% of the starting concentration, yielding a detection limit of about 100 nM. The data were collected on an Agilent Model 7890A GC equipped with VICI pulsed discharge detector**,** HP-PLOT/U column, inlet pressure of 10 psi, split ratio 100:1, oven temperature 120 °C. The calibration curve is used to measure the methanol concentration produced by bulk electrolysis. The Faradaic efficiency is given by: ([MeOH]*6e-)/i•t, where i•t is the integrated bulk electrolysis current.[5]

Chapter 4. Light-Driven CO_2 Reduction

4.1. Introduction

To alleviate earth atmosphere change and energy crisis, scientists have been studying CO_2 reduction for decades. The reduction is thermodynamically uphill, meaning it requires energy input. Obviously this energy can't come from fossil fuels, because that would produce more CO_2 than it would reduce. Therefore the ideal strategy is to use a non-fossil fuel source, preferably a renewable source, such as solar energy, wind, biomass, etc., to reduce CO_2, achieving a carbon-neutral energy cycle.

An artificial photosynthesis system usually consists of a light-capturing component to generate the electron-hole separation (such as quantum dots) or other photosensitizer (such as metalloporphyrins, ruthenium or rhenium complexes with bipyridine), catalysts or electron mediators, and sacrificial electron donors (e.g. ascorbic acid). While the majority of the artificial photosynthesis study has been focused on water splitting, CO_2 reduction has started to attract more attention recently.[1]

The ideal light-capturing component should be capable of absorbing the visible light as well as the UV light. The match of energy level is important as well. Take semiconductor materials for example: the conduction band of the semiconductor should be as close to the reduction potential of CO_2/related reduced products pair as possible. These two principles also apply for the choice of the photoelectrode in photoelectrochemical CO_2 reduction.

The Armstrong group observed fast CO_2 reduction driven by visible light using the assemblies of CdS nanocrystals with carbon monoxide dehydrogenase molecules.[2] In order to achieve photochemical CO_2 reduction using the PTE catalyst discussed in Chapter 3, we introduced CdSe quantum dots to the system. Besides quantum dots, we also tried other photosensitizers such as NADH and $Ru(bpy)_3^{2+}$. The scheme of the system is shown in Figure 4.1.

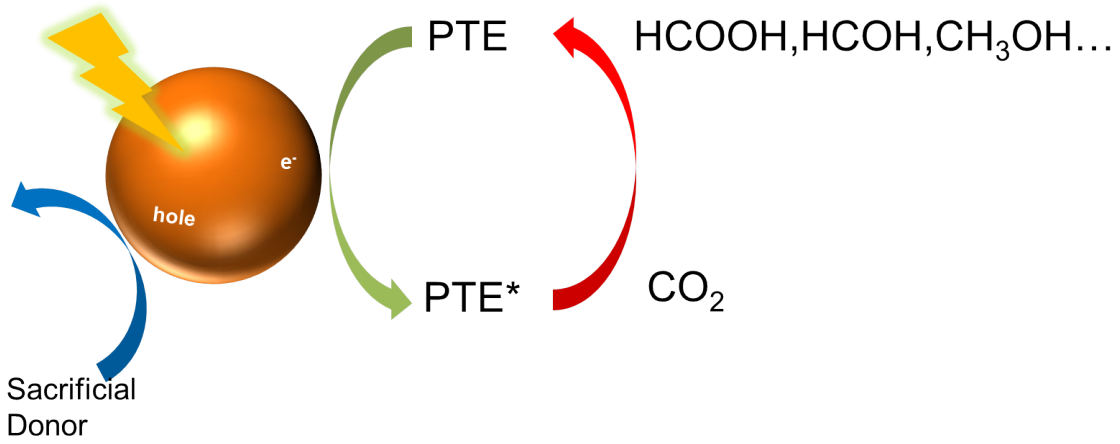

Figure 4.1. Scheme of photochemical CO_2 reduction system

4.2. Experiment

4.2.1. CdSe quantum dots synthesis

The synthesis of CdSe quantum dots followed the previous procedure.[3] TOPO (3.0g), ODPA (0.280g) and CdO (0.060g) are mixed in a flask, heated to 150°C and exposed to vacuum for 1 hour. The solution is then heated to above 300°C under nitrogen to dissolve

the CdO. When the solution turns optically clear and colorless, 1.5g of TOP is injected and the temperature is allowed to recover to the value required for the injection of the Se:TOP solution (0.058g Se + 0.360g TOP).

4.2.2. Transient absorbance spectroscopy

It is a pump probe experiment, in which a pump pulse is used to excite the sample and then a white light probe pulse is used to measure the transient absorbance. The time delay between the pump and probe pulses is varied to measure the time dependence of the absorbance spectrum.

4.2.2.1. Transient absorbance spectroscopy-Visible region

The transient absorbance spectroscpy in visible region was obtained on the set-up in Prof. Tianquan Lian lab. The set-up detail was described earlier.[4]

4.2.2.2. Transient absorbance spectroscopy-UV region

The scheme of the femtosecond transient absorbance spectroscpy in UV region set-up is shown in Figure 4.2. A BBO is used to generate 400 nm to be used as the seed for continuum generation. Calcium fluoride is used as the nonlinear crystal which generated the 270- 380 nm continuum which is then filtered with a short pass filter to get rid of the 400 nm pump. The OPA is used to generate the pump that is going to be used for excitation and passed through the delay line to be delayed. A chopper is used to chop the pump generating a pump on and off to obtain the delta absorbance. The continuum is focused at the sample and then collimated and refocused at the fiber for detection with the ocean optics spectrometer.

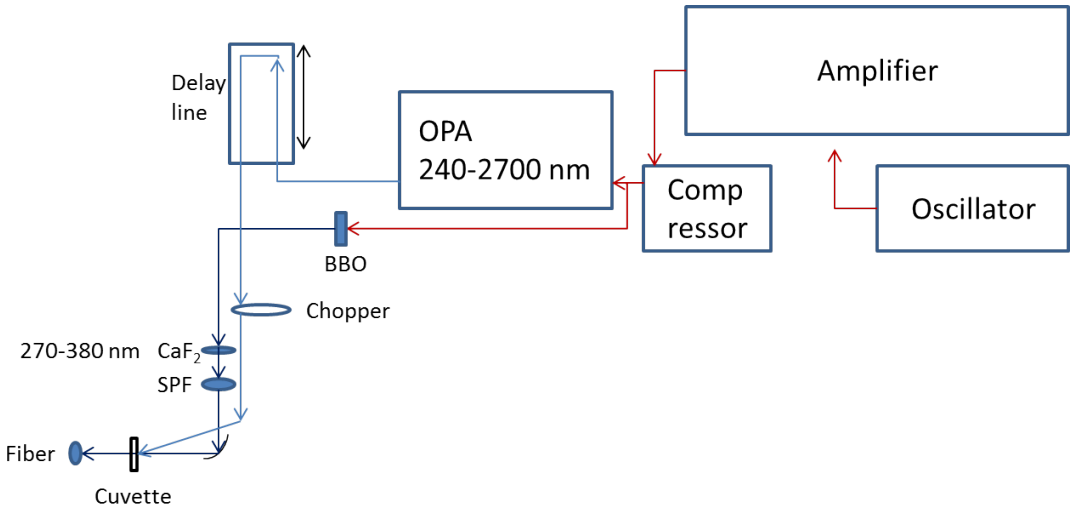

Figure 4.2. Femtosecond transient absorbance spectroscopy set-up

4.2.3. Spectroelectrochemistry

The spectroelectrochemistry was conducted in the SEC-C - 0.5 mm thin layer Quartz glass cell kit (PT) (BASi EF-1362). CV-50W potentialstat and Agilent 8453 UV-Vis spectrometer were used to get the electrochemistry and UV-Vis data at the same time. All of those instruments were from Prof. Craig L. Hill lab.

4.3. Results and dicusssion

4.3.1. UV-Vis spectroelectrochemistry

To better understand the spectroscopy features of PTE and its reduced form, we conducted UV-Vis spectroelectrochemistry. As shown in Figure 4.3b, in aqueous solution, when -600 mV is applied, the UV-Vis spectrum, which shows two major absorption peaks at 297 nm and 352 nm, has almost no change, indicating that PTE is not reduced yet. However, when -800 mV is applied, the peaks of 297 and 352 nm decreases gradually and there are positive features formed at 270 nm, 320 nm and 345 nm, which

are the absorption bands of 2 electron reduced PTE. Figure 4.3a is the difference spectrum (reduced PTE minus oxidized PTE), showing the bleaches at 297 nm and 352 nm and positive features at 270 nm and 320 nm. Changing to wet THF (H_2O as proton source) solvent (Figure 4.3c and 4.3d), the transition is similar but shows several obvious isosbestic points. The reduced PTE peaks red shift from the oxidized PTE peaks.

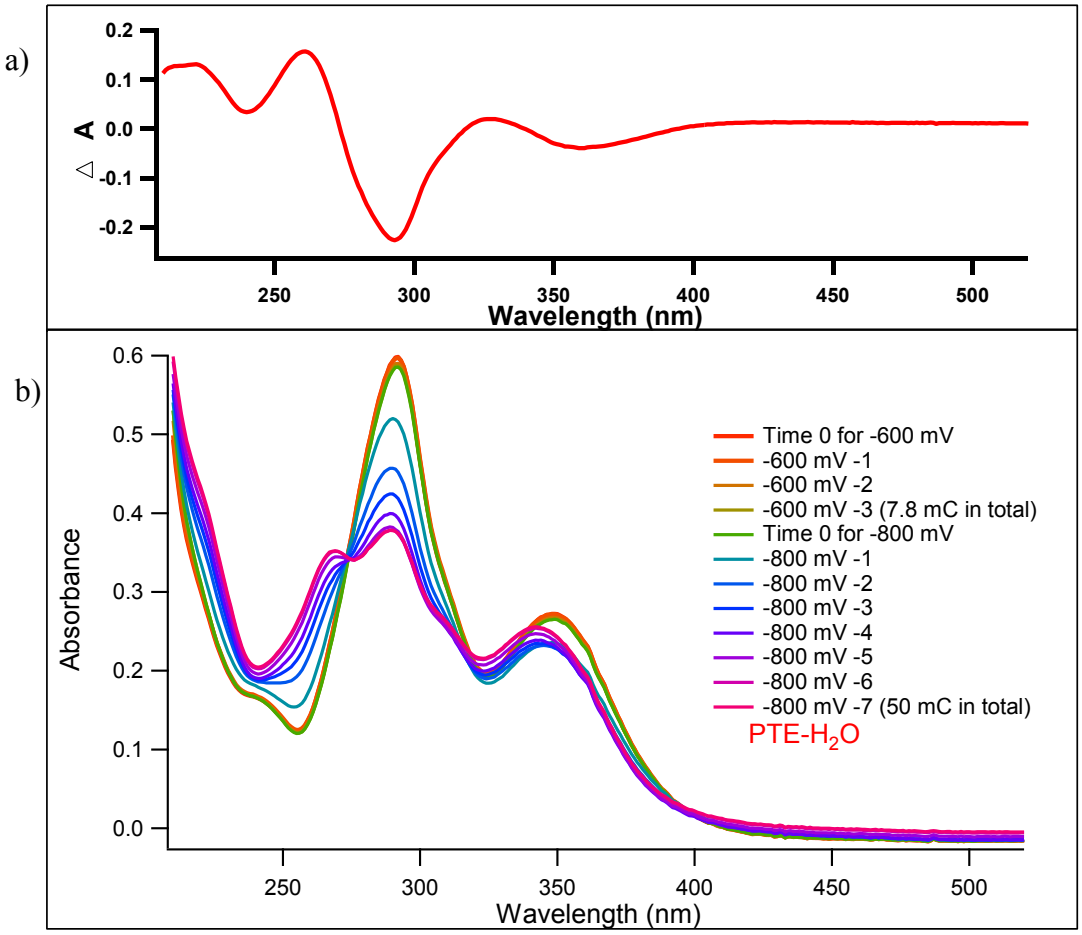

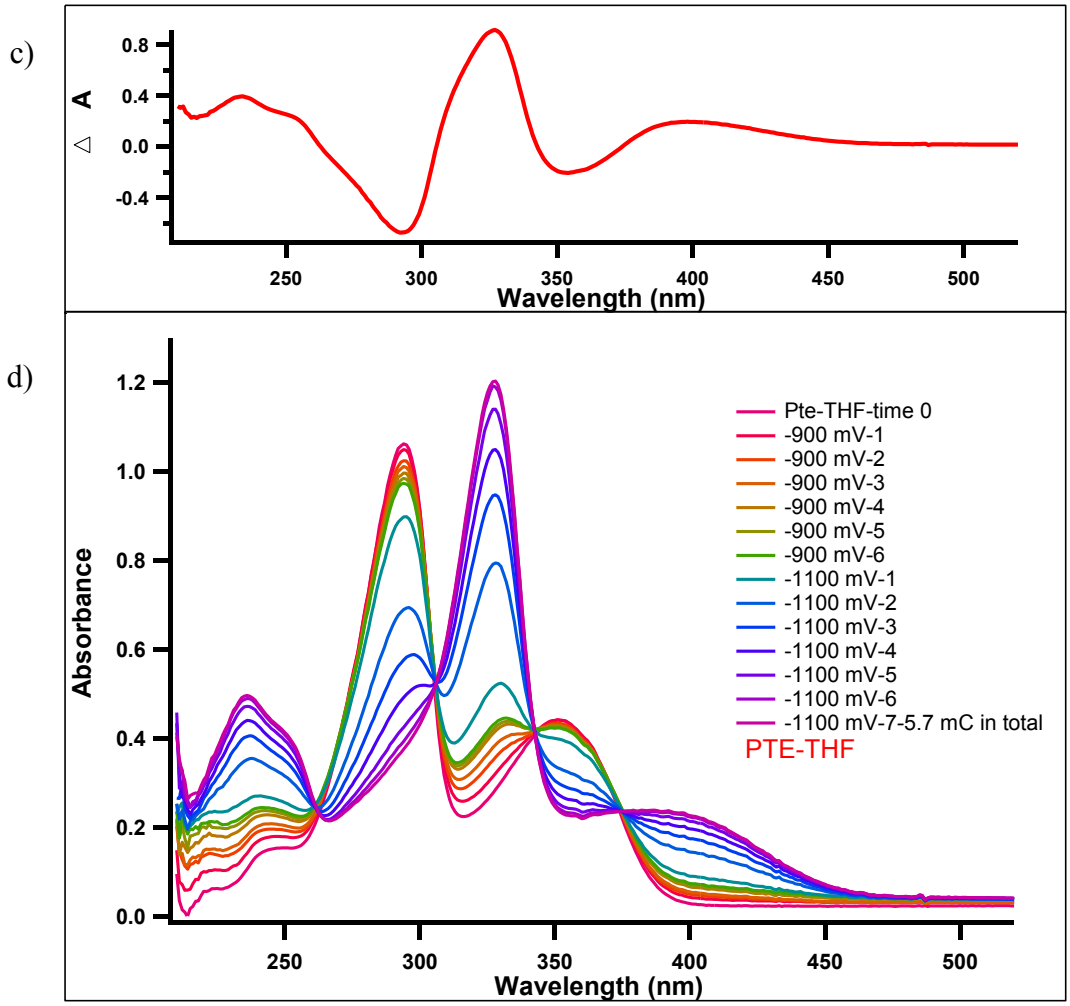

Figure 4.3. UV-Vis spectroelectrochemistry. Difference UV-Vis spectrum of reduced PTE and PTE in (a) H_2O. (c) Tetrahydrofuran (THF). The progression of UV-Vis spectrum under negative reducing potentials in (b) H_2O. (d) THF

4.3.2. PTE-quantum dots

A photoluminescence quenching experiment is shown in Figure 4.4. As the amount of PTE added into the CdSe quantum dots solution increases, the fluorescence intensity decreases gradually. When the ratio of PTE/QD is 13, there is 43% quenching. The Stern-Volmer plot in Figure 4.3c shows a linear fitting, indicating one process dominates (intermolecular quenching from the PTE interaction) the quenching. However, there are various processes which can result in quenching, such as excited state reactions, PTE-QD or other complex formation, collision, and energy transfer, so this experiment alone does not establish electron transfer from the QD to the PTE.

a)

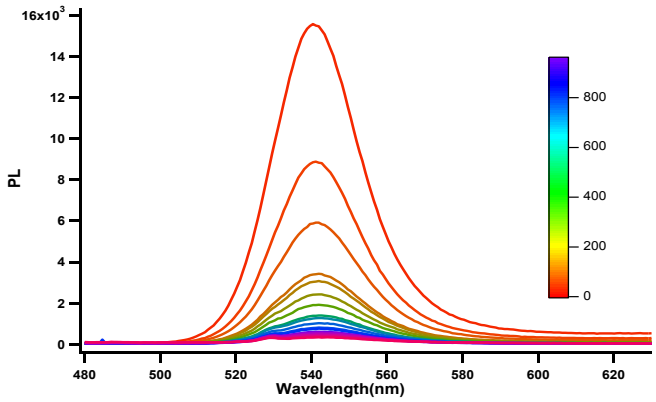

b)

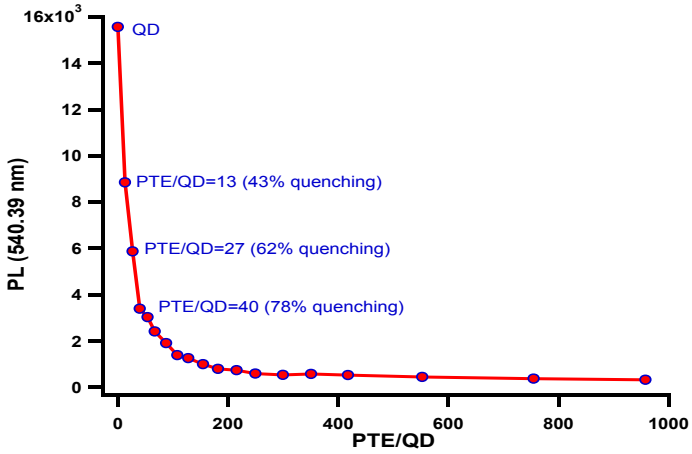

c)

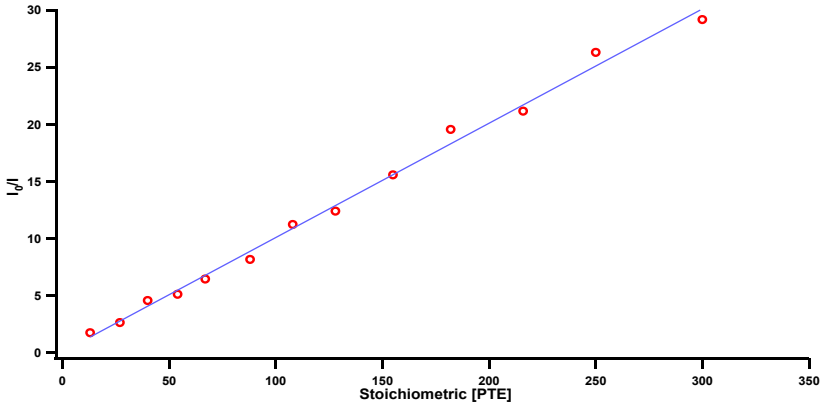

Figure 4.4. Photoluminescence quenching experiment. (a) Change of quantum dot photoluminescence with gradient addition of PTE. (b) Photoluminescence quenching based on the PTE/QD ratio. (c) Stern-Volmer plot.

The transient visible absorption spectroscopy data is shown in Figure 4.5 (analysis of 523-530 nm, QD 1S bleach). These spectra were taken under the same conditions with low excitation energy to ensure negligible populations in multiple exciton states. The 1S exciton bleach of QD decays relatively slowly, indicating long-lived electrons in the 1S level and negligible multiple excitons under this low excitation energy. When PTE is added, the 1S exciton bleach recovers to half its initial value within 100 ps, suggesting short-lived 1S electrons. There are various pathways for the electron, including electron trapping and electron transfer.

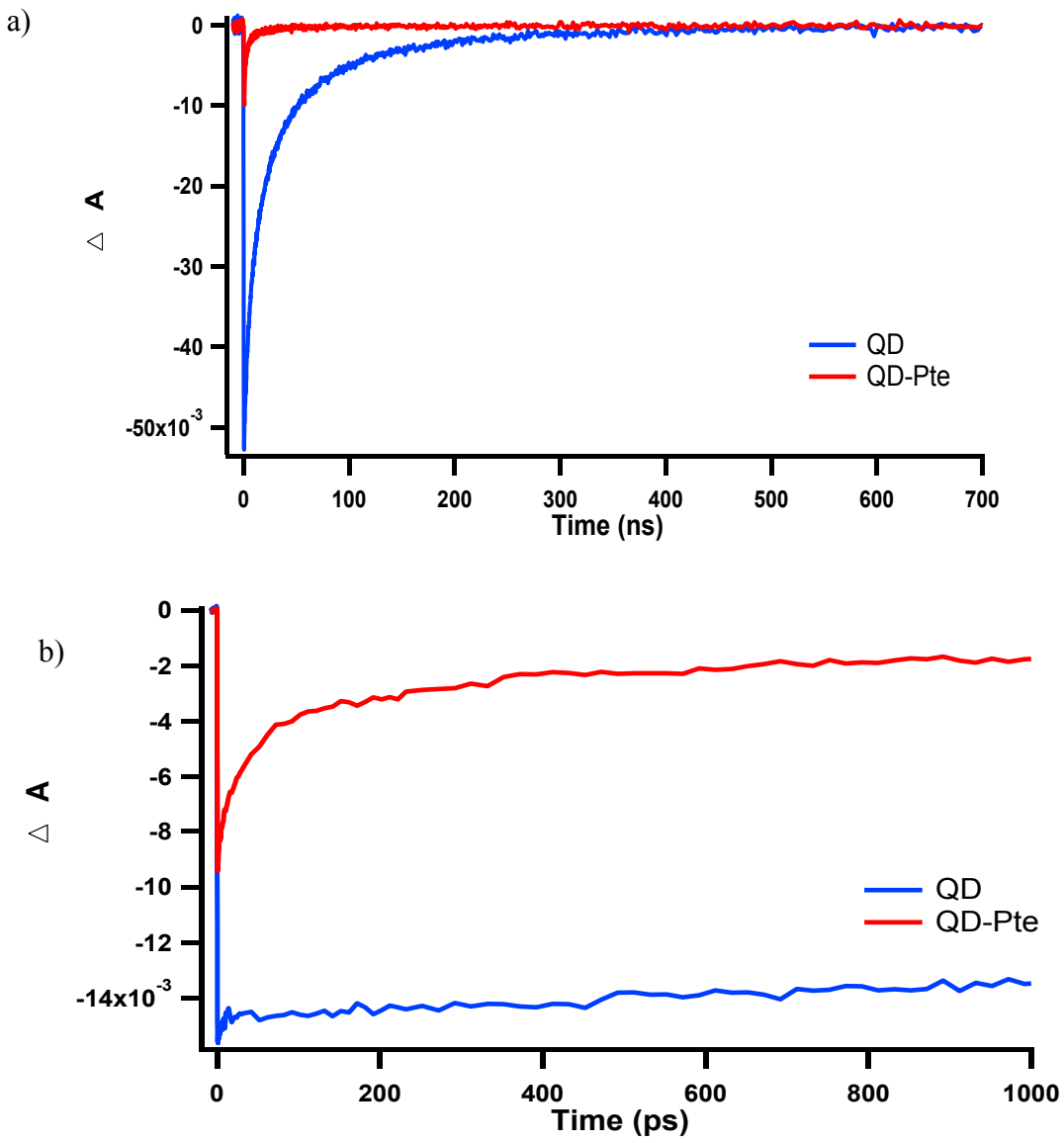

Figure 4.5. Transient visible absorption spectroscopy. Comparison of the recovery kinetics of QD 1S exciton bleach in CdSe and CdSe-PTE systems. (a) nanosecond timescale. (b) picosecond timescale

Both the photoluminescence quenching and transient visible absorption spectroscopy have multiple possible explanations, even though electron transfer from QD to PTE is

included. Therefore, neither of those two experiments provides direct evidence for electron transfer from QD to PTE. To better understand the process, we conducted transient UV absorption spectroscopy, as shown in Figure 4.6. This is a separate experimental setup that uses 400 nm light to generate the continuum, in order to produce enough UV probe light for the experiment. Wet THF is used in order to provide proton. Figure 4.6a shows negligible change in UV region when there is only QD present. When PTE is added (Figure 4.6b), there is a bleach at 320 nm, indicating the decrease of the ground state PTE.

However, comparing this transient UV absorption spectra data (Figure 4.6) with the UV-Vis electrochemistry data (Figure 4.3), we found that the bleach is at different positions, which can be explained by the difference of 1 e^- (TA) and 2 e^- (electrochemistry) reduction. As aforementioned (Chapter 1&3), the active form of PTE as a catalyst is the 2 e^- reduced species. Thus, to achieve photochemical CO_2 reduction in this QD-PTE system, the PTE should be 2 e^- reduced by electrons transferred from QD, which is still quite challenging at present. One possibility is that some 2 e^- will be generated over time because of the disproportion of the 1 e^- reduced species. This will be diffusion limited, so it will happen on longer timescales which is why we did not see it in the ultrafast experiment.

a)

b)

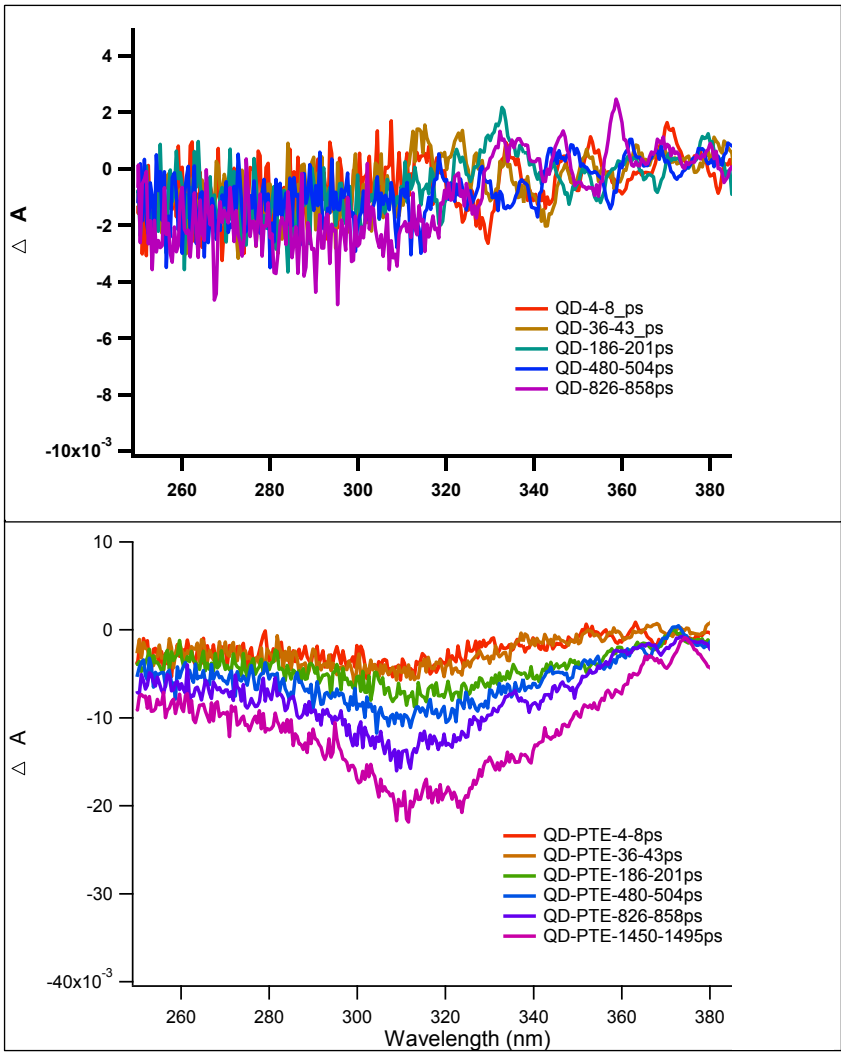

Figure 4.6. Transient UV absorption spectroscopy of (a) CdSe QD. (b) CdSe QD-PTE

4.3.3. Other photosensitizer (NADH, $Ru(bpy)_3^{2+}$)

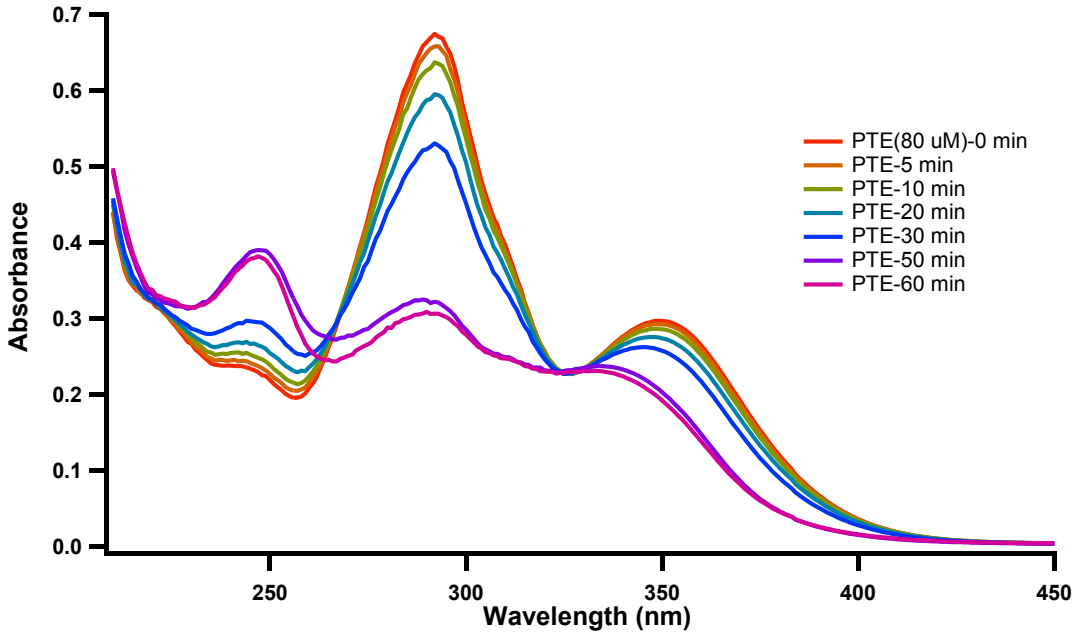

Figure 4.7. UV-Vis spectra of PTE under 351 nm illumination

Thus, we tried other photosensitizers to replace QD's including NADH and $Ru(bpy)_3^{2+}$. Figure 4.7 shows the UV-Vis spectra of PTE under 351 nm illuminations (where NADH has strong absorption). The absorption of PTE decreases rapidly, suggesting a decomposition of PTE under this 351 nm illumination, which is reasonable because PTE also has strong absorbance in UV region.

$Ru(bpy)_3^{2+}$ is also a common photosensitizer. As discussed in chapter 3, PTE(II), as another pterin derivative, is also a potential catalyst for CO_2 reduction. We used PTE(II)

in this system. Ethylenediaminetetraacetic acid (EDTA) is used as sacrificial donor. In Figure 4.8b, for the solution pre-saturated by CO_2, FTIR shows the bleach of PTE(II) and possible product formation. However, the positive features in the control experiment of Ar are still puzzling. This experiment is conducted in a sealed FTIR copper cell in N_2 purged box, and water vapor is an important factor to influence quality of the spectrum. Even though the results are not clean, it still suggests the difference between the system of Ar and CO_2. Further study should be conducted.

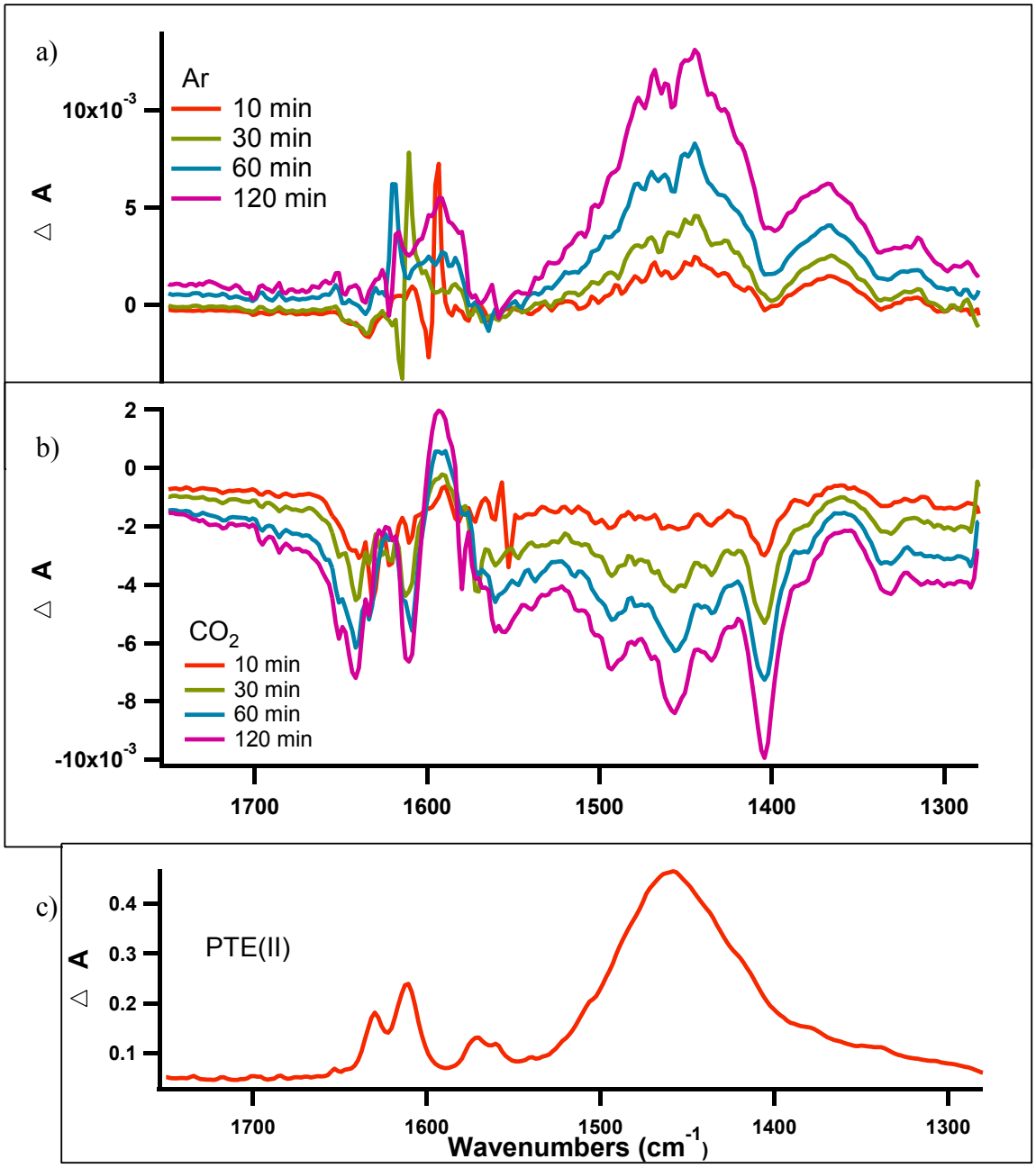

Figure 4.8. In situ FTIR. FTIR spectra at different illumination time of PTE (II) (a) Ar pre-saturated solution. (b) CO_2 pre-saturated solution. (c) FTIR spectrum of PTE(II). $Ru(bpy)_3^{2+}$ as photosensitizer, EDTA as sacrificial donor, 527 nm illumination

4.4. Conclusion

Multiple system have been tried to capture light to achieve the photochemical reduction of CO_2 including CdSe quantum dots, NADH, and $Ru(bpy)_3^{2+}$. However, it is still challenging to get the 2 e^- reduced form of PTE photochemically, which is the active form to catalyze CO_2 reduction.

References

1. (a) Qiu, J.; Zeng, G.; Ha, M.-A.; Ge, M.; Lin, Y.; Hettick, M.; Hou, B.; Alexandrova, A. N.; Javey, A.; Cronin, S. B., Artificial Photosynthesis on TiO_2-Passivated InP Nanopillars. *Nano Lett* **2015,** *15* (9), 6177-6181; (b) Bachmeier, A.; Hall, S.; Ragsdale, S. W.; Armstrong, F. A., Selective Visible-Light-Driven CO_2 Reduction on a p-Type Dye-Sensitized NiO Photocathode. *J Am Chem Soc* **2014,** *136* (39), 13518-13521; (c) Bachmeier, A.; Wang, V. C. C.; Woolerton, T. W.; Bell, S.; Fontecilla-Camps, J. C.; Can, M.; Ragsdale, S. W.; Chaudhary, Y. S.; Armstrong, F. A., How Light-Harvesting Semiconductors Can Alter the Bias of Reversible Electrocatalysts in Favor of H_2 Production and CO_2 Reduction. *J Am Chem Soc* **2013,** *135* (40), 15026-15032; (d) Kumar, B.; Llorente, M.; Froehlich, J.; Dang, T.; Sathrum, A.; Kubiak, C. P., Photochemical and Photoelectrochemical Reduction of CO_2. *Annual Review of Physical Chemistry, Vol 63* **2012,** *63*, 541-+; (e) Sato, S.; Arai, T.; Morikawa, T.; Uemura, K.; Suzuki, T. M.; Tanaka, H.; Kajino, T., Selective CO_2 Conversion to Formate Conjugated with H_2O Oxidation Utilizing Semiconductor/Complex Hybrid Photocatalysts. *J Am*

Chem Soc **2011,** *133* (39), 15240-15243; (f) Sato, S.; Morikawa, T.; Saeki, S.; Kajino, T.; Motohiro, T., Visible-Light-Induced Selective CO_2 Reduction Utilizing a Ruthenium Complex Electrocatalyst Linked to a p-Type Nitrogen-Doped Ta_2O_5 Semiconductor. *Angewandte Chemie International Edition* **2010,** *49* (30), 5101-5105; (g) Parkinson, B. A.; Weaver, P. F., Photoelectrochemical pumping of enzymatic CO_2 reduction. *Nature* **1984,** *309* (5964), 148-149.

2. Chaudhary, Y. S.; Woolerton, T. W.; Allen, C. S.; Warner, J. H.; Pierce, E.; Ragsdale, S. W.; Armstrong, F. A., Visible light-driven CO_2 reduction by enzyme coupled CdS nanocrystals. *Chem Commun* **2012,** *48* (1), 58-60.

3. Carbone, L.; Nobile, C.; De Giorgi, M.; Sala, F. D.; Morello, G.; Pompa, P.; Hytch, M.; Snoeck, E.; Fiore, A.; Franchini, I. R.; Nadasan, M.; Silvestre, A. F.; Chiodo, L.; Kudera, S.; Cingolani, R.; Krahne, R.; Manna, L., Synthesis and micrometer-scale assembly of colloidal CdSe/CdS nanorods prepared by a seeded growth approach. *Nano Lett* **2007,** *7* (10), 2942-2950.

4. Wu, K.; Chen, Z.; Lv, H.; Zhu, H.; Hill, C. L.; Lian, T., Hole Removal Rate Limits Photodriven H_2 Generation Efficiency in CdS-Pt and CdSe/CdS-Pt Semiconductor Nanorod–Metal Tip Heterostructures. *J Am Chem Soc* **2014,** *136* (21), 7708-7716.

Chapter 5. Summary

We studied pyridine, pteridine and their derivatives as catalysts for CO_2 reduction. PTE can reduce CO_2 catalytically on glassy carbon electrode with low overpotential, without any involvement of metals. Formate, formaldehyde and methanol are detected as products by FTIR, gas chromatography and NMR. The yield of methanol is modest. One of the reason is that PTE catalyst lacks the extended substituent at position 6 of the pyrazine ring normally present in methanogenic cofactors such as MPT.[1] Therefore PTE cannot stabilize a cyclic methylene intermediate, which may limit the efficiency of further reduction steps beyond the first two-electron reduction to formate.

PTE-CO_2 is proposed as an intermediate based on the FTIR data, and followed by hydride transfer-proton transfer process based on the analogy of biological system[2] and theoretical studies.[3] Reduction in 2 e^- steps by hydride transfer avoids high energy intermediates. The hydride transfer is likely facilitated by rearomatization of the pyrazine ring. Future work to explore the mechanism should focus on direct verification of the hydride transfer mechanism.

Photochemical CO_2 reduction using PTE is still challenging. The active form of PTE for catalysis is the two-electron reduced PTE. However, PTE can be only one-electron reduced by electron transfer from CdSe quantum dots. Future work can focus on how to produce two-electron reduced PTE photochemically.

Reference

1. Dimarco, A. A.; Bobik, T. A.; Wolfe, R. S., Unusual Coenzymes of Methanogenesis. *Annu Rev Biochem* **1990,** *59*, 355-394.

2. Maden, B. E. H., Tetrahydrofolate and tetrahydromethanopterin compared: functionally distinct carriers in C-1 metabolism. *Biochem J* **2000,** *350*, 609-629.

3. (a) Lim, C. H.; Holder, A. M.; Hynes, J. T.; Musgrave, C. B., Catalytic Reduction of CO_2 by Renewable Organohydrides. *J Phys Chem Lett* **2015,** *6* (24), 5078-5092; (b) Lim, C. H.; Holder, A. M.; Hynes, J. T.; Musgrave, C. B., Reduction of CO_2 to Methanol Catalyzed by a Biomimetic Organo-Hydride Produced from Pyridine. *J Am Chem Soc* **2014,** *136* (45), 16081-16095.